ULTRAFAST SPECTROSCOPY IN CONDENSED PHASE: STUDY OF POLAR SOLVATION AND EXCITON FISSION

PANKAJ SELIYA

A dissertation submitted for the partial fulfilment of Master of Science (MS) degree in Chemical Sciences

INDIAN INSTITUTE OF SCIENCE EDUCATION AND RESEARCH MOHALI

April 2019

ULTRAFAST SPECTROSCOPY IN CONDENSED PHASE: STUDY OF POLAR SOLVATION AND EXCITON FISSION

PANKAJ SELIYA

MP16005

A dissertation submitted for the partial fulfilment of Master of Science (MS) degree in Chemical Sciences

INDIAN INSTITUTE OF SCIENCE EDUCATION AND RESEARCH MOHALI

April 2019

CERTIFICATE OF EXAMINATION

This is to certify that the dissertation titled "**Ultrafast spectroscopy in condensed phase: study of polar solvation and exciton fission"** submitted by **Mr. Pankaj Seliya** (Reg. No. MP16005) for the partial fulfilment of MS degree programme of the Institute, has been examined by the thesis committee duly appointed by the Institute. The committee finds the work done by the candidate satisfactory and recommends that the report be accepted.

Prof. K.S. Viswanathan Dr. Jino George Dr. Arijit Kumar De
(Supervisor)

Date: April 26, 2019

DECLARATION

The work presented in this dissertation has been carried out by me under the guidance of Dr. Arijit Kumar De at the Indian Institute of Science Education and Research Mohali.

This work has not been submitted in part or in full for a degree, a diploma, or a fellowship to any other university or institute. Whenever contributions of others are involved, every effort is made to indicate this clearly, with due acknowledgement of collaborative research and discussions. This thesis is a bonafide record of original work done by me and all sources listed within have been detailed in the bibliography.

Pankaj Seliya

(Candidate)

Date: April 26, 2019

In my capacity as the supervisor of the candidate's project work, I certify that the above statements by the candidate are true to the best of my knowledge.

Dr. Arijit Kumar De

(Supervisor)

ACKNOWLEDGEMENTS

First of all, I would like to thank Dr. Arijit Kumar De for providing me with interesting problems to work on and for the insightful discussions to solve them.

I would like to thank Prof. K.S. Viswanathan, Dr. Jino George and Dr. K.R. Shamasundar for their valuable scientific comments which provided great help in the project.

I would like to thank Ms. Yogita Silori for helping me in doing the experiments. I would also like to thank my lab members Dr. Arindam Das, Dr. Subhash Chander, Ms. Anita Devi, Ms. Shaina Dhamija, Mr. Sumit Yadav, Ms. Garima Bhutani, Ms. Sakshi Chawla, Mr. Ajeet Kumar, Ms. Shruthi S. Nair and Ms. Umang Gupta for their constant support, inspiration and fruitful discussions.

I would like to thank IISER Mohali for all the instrumentation facilities and the library for providing access to a plethora of journals.

And finally, to my friends and family for their constant motivation and support.

CONTENTS

LIST OF FIGURES

ABBREVIATIONS

TAS:	Transient Absorption Spectroscopy
SE:	Stimulated Emission
GSB:	Ground State Bleach
ESA:	Excited State Absorption
SF:	Singlet Fission
NOPA:	Noncollinear Optical Parametric Amplifier
BBO:	Beta Barium Borate (BaB_2O_4)
2DES:	Two-Dimensional Electronic Spectroscopy
S_R:	Rephasing Signal
S_{NR}:	Non – Rephasing Signal
FT:	Fourier Transformation
PC:	Phase Cycling
DSFD:	Double Sided Feynman Diagram
TPA:	Two Photon Absorption
OPA:	One Photon Absorption
FWHM:	Full Width at Half Maxima
SHG:	Second Harmonic Generation
FROG:	Frequency Resolved Optical Gating

ABSTRACT

In condensed phase, the system under study does not only show its own property but also evolves as a function of its interaction with the surroundings.

In first part, the interaction of system (solute) with its environment (solvent) is studied. We have studied how the interaction of a chromophore with a polar solvent relaxes the excited state of the chromophore. The sub 1ps dynamics of relaxation are studied for two solvents (ethanol and ethylene glycol) using the technique of TAS and 2DES.

In second part, the interaction of a chromophore molecule with the neighboring chromophore of same type is studied. In polyacene molecules (such as tetracene and pentacene); one of the outcomes of such interaction is the formation of pair of triplets from a singlet exciton called as singlet fission. Using the technique of TAS, we have studied that while pentacene shows very robust singlet fission, the singlet fission in case of tetracene is not very robust. Also, the role of vibrational states in the singlet fission of pentacene have been studied.

THESIS AT A GLANCE

This thesis is composed of three different sections. Each section has been briefly described below and a detailed description can be found in the dedicated chapters.

The first section consists of characterization of the laser pulses and the techniques employed to study the dynamics of the systems. The employed techniques are transient absorption spectroscopy (TAS) and two – dimensional electronic spectroscopy (2DES). While Both the techniques are useful in studying the dynamics in sub – ps regime, 2DES has an extra advantage of frequency resolving the excitation axis and helps to resolve the overlapping molecular responses.

The second section involves the study of polar solvation under 1 ps of two solvents (ethanol and ethylene glycol) using the techniques of TAS and 2DES. Using TAS, correlation function can be drawn without the need of indirect reconstruction of emission spectra. Apart from studying the sub 1 ps dynamics, 2DES is also employed to construct the excitation wavelength dependent correlation function which is not possible with the help of fs-TAS.

The third section reports the excited state Photophysics in two different kinds of systems. The first is the studying the excited state dynamics in Polyacenes (tetracene and pentacene). One of the most intriguing process that takes places in these molecules is singlet fission where one the excited singlet can share its energy with a neighboring chromophore to generate a pair of triplets. The study reveals that tetracene (in toluene solution) doesn't undergo a robust singlet fission but pentacene (in thin film) can undergo very robust singlet fission at room temperature. It has been shown that the singlet fission in pentacene takes place within 200 fs and there is a direct involvement of the vibrational states of the triplet during singlet fission.
Apart from studying the dynamics of Polyacenes, two photon studies in Rhodamine 6G solution are also carried out which reveals the states are inaccessible using the linear absorption spectroscopy.

Techniques

1. **Pulse Characterization**

2. **Transient Absorption Spectroscopy**

3. **Two-Dimensional Electronic Spectroscopy**

Pulse Characterization

1.1.Calculation of spectral width

The spectrum of the output of Ti: Sapphire amplifier (Libra, Coherent) was measured using Ocean Optics Spectrometer. The spectrum of the laser with Gaussian fitting is shown in figure (1.1).

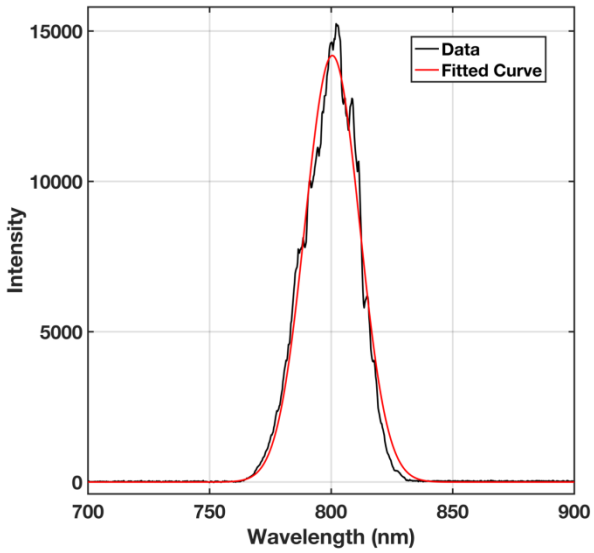

Figure 1.1: Spectrum of the output of Ti: Sapphire amplifier

The laser spectrum was fitted to a Gaussian equation (equation (1.1))

$$\mathbf{y = a \times \exp\left(\frac{-4\times \ln(2)\times(x-b)^2}{w^2}\right)} \qquad \mathbf{(1.1)}$$

Where, a = height of fitted Gaussian; b = center of fitted Gaussian; w = full-width at half maximum (FWHM)

The values for the fitting parameters obtained are:

a = 14180 units; b = 800.5 nm; w = 26.41 nm

The FWHM for the fitted Gaussian is 26.41 nm. Therefore, the spectral width of the laser is 26.41 nm.

1.2. Calculation of Fourier transform limited pulse width

For a Gaussian pulse, the Fourier transform relation is [1]:

$$\Delta\boldsymbol{\omega}.\Delta\mathbf{t} = \mathbf{2.772} \text{ Or } \Delta\boldsymbol{\nu}.\Delta\mathbf{t} = \mathbf{0.441} \tag{1.2}$$

Spectral width of the laser = 26.41 nm

$$\Delta\boldsymbol{\lambda} = \mathbf{26.41\ nm}; \boldsymbol{\lambda} = \mathbf{800.5\ nm};$$

$$\mathbf{c = speed\ of\ light\ in\ vacuum = 300\ nm\ fs^{-1}}$$

$$\mathbf{h\nu} = \frac{\mathbf{hc}}{\boldsymbol{\lambda}} \tag{1.3}$$

$$\Delta\boldsymbol{\nu} = -\frac{\mathbf{c}}{\boldsymbol{\lambda^2}} \times \Delta\boldsymbol{\lambda} \tag{1.4}$$

$$|\Delta\boldsymbol{\nu}| = \frac{\mathbf{c}}{\boldsymbol{\lambda^2}} \times \Delta\boldsymbol{\lambda} = \frac{\mathbf{300\ nm\ fs^{-1} \times 26.41\ nm}}{\mathbf{(800.5)^2\ nm^2}} = \mathbf{0.0124\ fs^{-1}}$$

Using equation (1.2),

$$\Delta\mathbf{t} = \frac{\mathbf{0.441}}{\Delta\boldsymbol{\nu}} \tag{1.5}$$

$$\Delta\mathbf{t} = \frac{\mathbf{0.441}}{\mathbf{0.0124}}\ \mathbf{fs} = \mathbf{35.7\ fs}$$

Therefore, the Fourier transform limited pulse width is 35.7 fs.

1.3. Intensity Autocorrelation

In an intensity autocorrelation, the laser beam is split into two pulses using a beam splitter. The delay between the two pulses is varied using a mechanical delay stage and the pulses are then combined non-collinearly inside a nonlinear crystal (e.g. BBO) to generate a signal at twice the frequency of input pulse. The second harmonic signal is recorded as a function of delay between the two pulses [1] & [2]. The intensity of second harmonic signal is high when the two pulses overlap in time inside the nonlinear crystal. Thus, the intensity of the second harmonic signal as function of delay between the pulses gives the information about the pulse width.

The intensity autocorrelation is given as:

$$\mathbf{A^2(\tau) \propto \int_{-\infty}^{\infty} I(t)I(t-\tau)\,dt} \tag{1.6}$$

For a Gaussian pulse, the autocorrelation width ($\Delta\tau$) is related to the pulse width (Δt) by the relation:

$$\frac{\Delta\tau}{\Delta t} = 1.414 \tag{1.7}$$

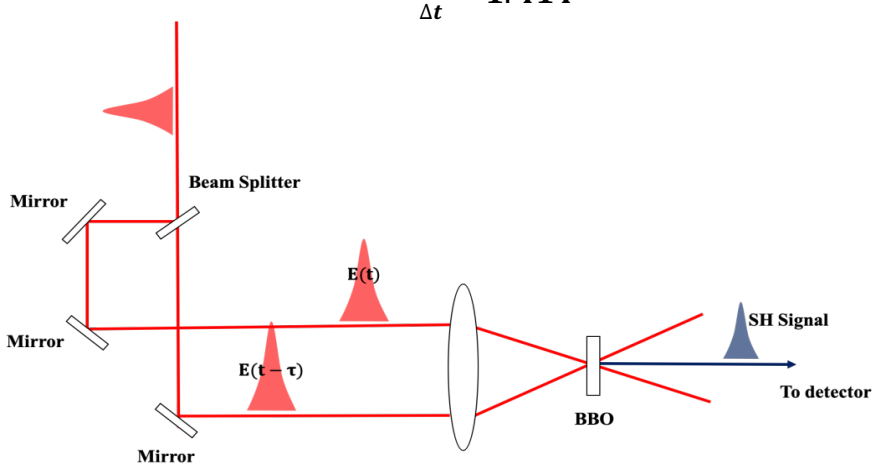

Figure 1.2: Second harmonic intensity autocorrelation setup

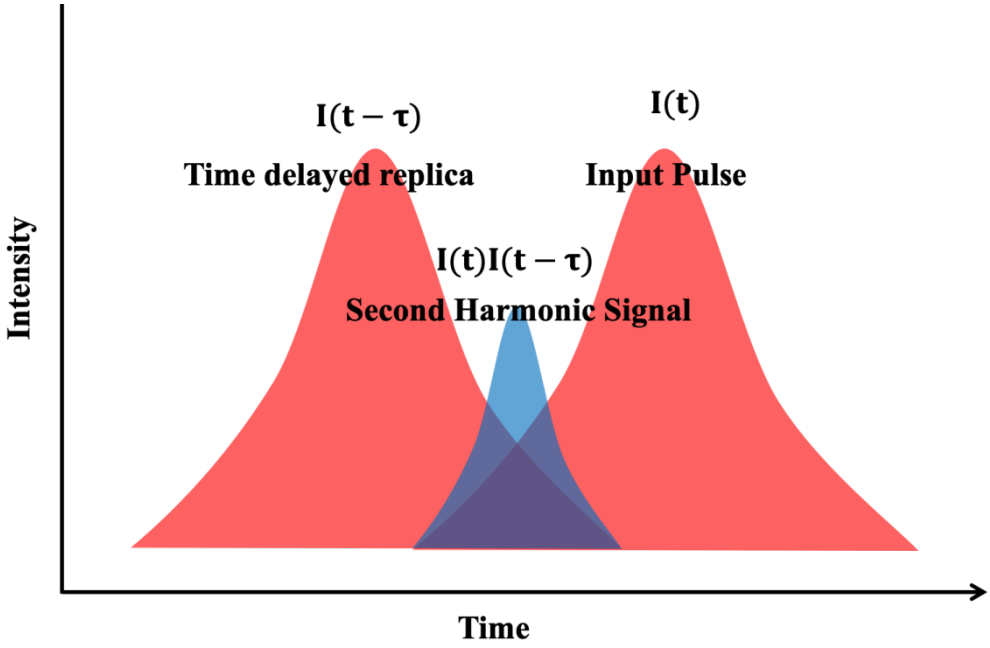

Figure 1.3: Intensity of second harmonic signal as a function of delay between the pulses

The autocorrelation trace of the 800 nm laser pulse was measured second harmonic intensity autocorrelation employing BBO as a nonlinear medium. The generated SH signal is shown in figure (1.4).

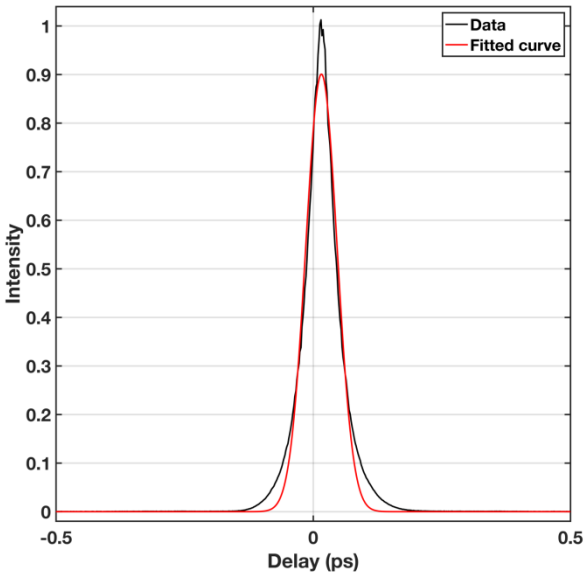

Figure 1.4: Autocorrelation trace of the output of Ti: Sapphire amplifier

The autocorrelation trace of the laser was fitted to a Gaussian (equation (1.1)) and the values of obtained fitting parameters are:

a = 0.90 units; b = 0.015 ps; w = 0.072 ps = 72 fs

Therefore, the autocorrelation width is 72 fs.
Since, the autocorrelation width and pulse width are related by equation (1.7), therefore the pulse width is:

$$\Delta t = \frac{72}{1.414}\ \text{fs} \approx 51\ \text{fs}$$

Therefore, the pulse width obtained using intensity autocorrelation is 51 fs.

Although intensity autocorrelation can provide the pulse width but it cannot provide any information about the phase in the pulse. Also, intensity autocorrelation is symmetric with respect to time so it cannot provide any information about the direction of time of a pulse.

1.4.Frequency resolved Optical gating

For complex pulses, intensity autocorrelation does not reveal complete information about the pulse. So, a different technique called as Frequency resolved Optical Gating (FROG) [3] is used to characterize the pulse which not only reveals the true temporal width of a laser pulse but also gives information about the spectral phase in the pulse. There are a number of variations of FROG technique but the one employed by us is called as the Second

Harmonic Generation FROG (SHG-FROG). The experimental setup for SHG – FROG is similar to SH intensity autocorrelation but instead of collecting the total intensity of SH signal using a single pixel detector, the SH signal is spectrally resolved using a spectrometer.

The spectrograph obtained as a function of wavelength and delay between the two replicas can be used to obtain the phase of the pulse using retrieval algorithm. The retrieval software used by was the one provided by Prof. Rick Trebino.

The characterization of the output of the amplifier using FROG is shown in figure (1.5).

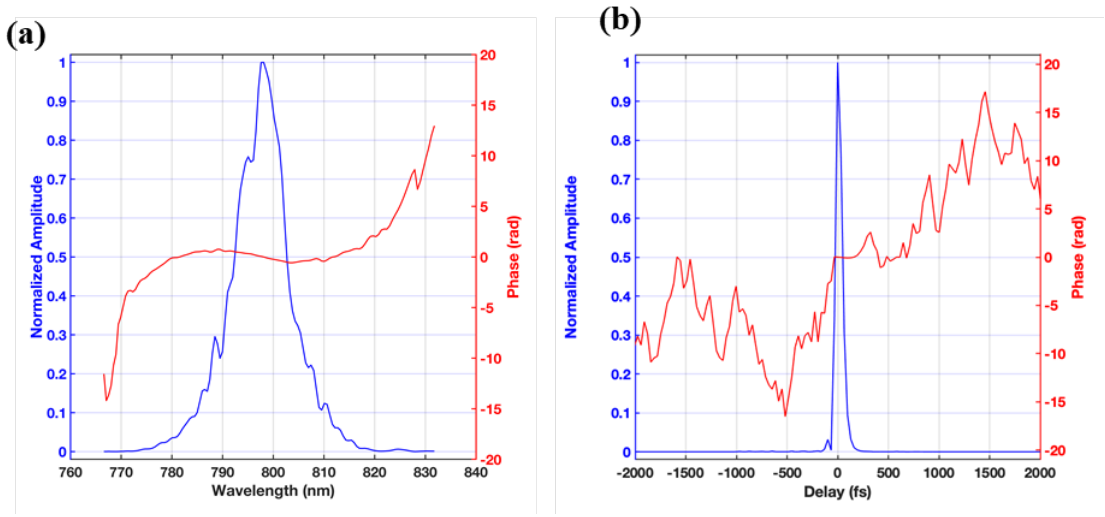

Figure 1.5: Phase of amplifier pulse (a) in frequency domain & (b) time domain retrieved using FROG

From figure (1.5(a)), it can be seen that the laser pulse predominantly has a third order (or cubic) phase present it because of which the true pulse width is greater than the transform limited pulse width. Pulse compression techniques such as using prism pairs can be used to compress the pulse to transform limited.

Transient Absorption Spectroscopy

Transient absorption spectroscopy (Pump-probe) is a time-resolved technique which is used to study transient absorption changes in the sample of interest. In a pump-probe experiment, the sample is first excited with an ultrashort laser pulse. Another pulse is introduced after some time which measures the changes in the sample created by the first pulse. The first pulse is called as the pump pulse and the second pulse is called as the probe pulse. The pump should have higher power as compared to the probe pulse because probe should not induce any changes in the sample and should only measure the changes created by the pump pulse. The time of arrival of the second pulse w.r.t. the first pulse is varied using a retroreflector placed on a mechanical delay line such that the entire time dependence of absorption could be studied.

Further, a chopper is introduced into the pump arm running at half the frequency of the laser such that every alternate pump pulse is blocked. The transmission of the probe is then taken both in presence of the pump and in absence of the pump. The difference of these two transmissions (or absorbance) gives the required transient absorption signal.

The pump beam is blocked after the sample and the intensity the probe is measured.

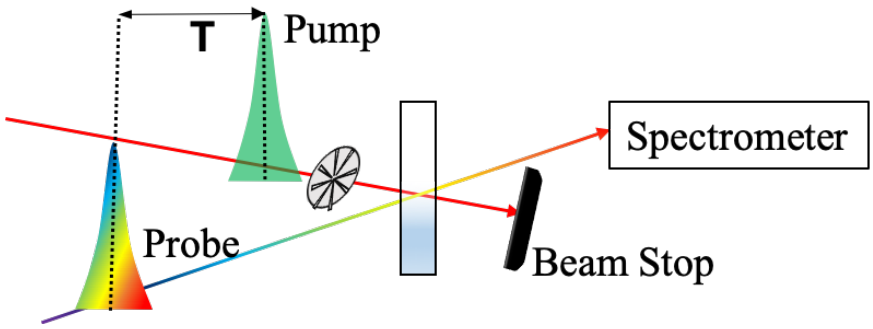

Figure 2.1: Schematic of a pump – probe experiment

Intensity of the probe transmitted when the pump is on:

$$\mathbf{I_{pump\ on} = I_0 \times 10^{-A_{pump\ on}}} \qquad \mathbf{(2.1)}$$

Taking logarithm on both sides:

$$\log(I_{pump\ on}) = \log(I_0) - A_{pump\ on} \quad (2.2)$$

$$A_{pump\ on} = \log(I_0) - \log(I_{pump\ on}) \quad (2.3)$$

I_0 = intensity of the incident pulse

$A_{pump\ on}$ = absorbance of probe pulse by sample in presence of the pump

Intensity of the probe transmitted when the pump is off:

$$I_{pump\ off} = I_0 \times 10^{-A_{pump\ off}} \quad (2.4)$$

Taking logarithm on both sides:

$$\log(I_{pump\ off}) = \log(I_0) - A_{pump\ off} \quad (2.5)$$

$$A_{pump\ off} = \log(I_0) - \log(I_{pump\ off}) \quad (2.6)$$

$A_{pump\ off}$ = absorbance of probe pulse by sample in absence of the pump

Subtracting equation (2.6) from equation (2.3) gives:

$$\Delta A = A_{pump\ on} - A_{pump\ off} = -\log(I_{pump\ on}) + \log(I_{pump\ off}) \quad (2.7)$$

$$\Delta A = \log\left(\frac{I_{pump\ off}}{I_{pump\ on}}\right) \quad (2.8)$$

ΔA = measured differential absorption signal

The intensity of the probe is measured using grating based spectrometer which resolves the wavelengths in the signal.

The measured differential absorption signal is thus a function of both delay time (t) between the pump and the probe and wavelengths (λ) in the probe.

$$\Delta A = \Delta A(t, \lambda) \quad (2.9)$$

2.1. Transient absorption signal

The transient absorption signal of a molecule can contain three types of signals which are: (1) Ground State Bleach (GSB) (2) Stimulated Emission (SE) (3) Excited State Absorption (ESA).

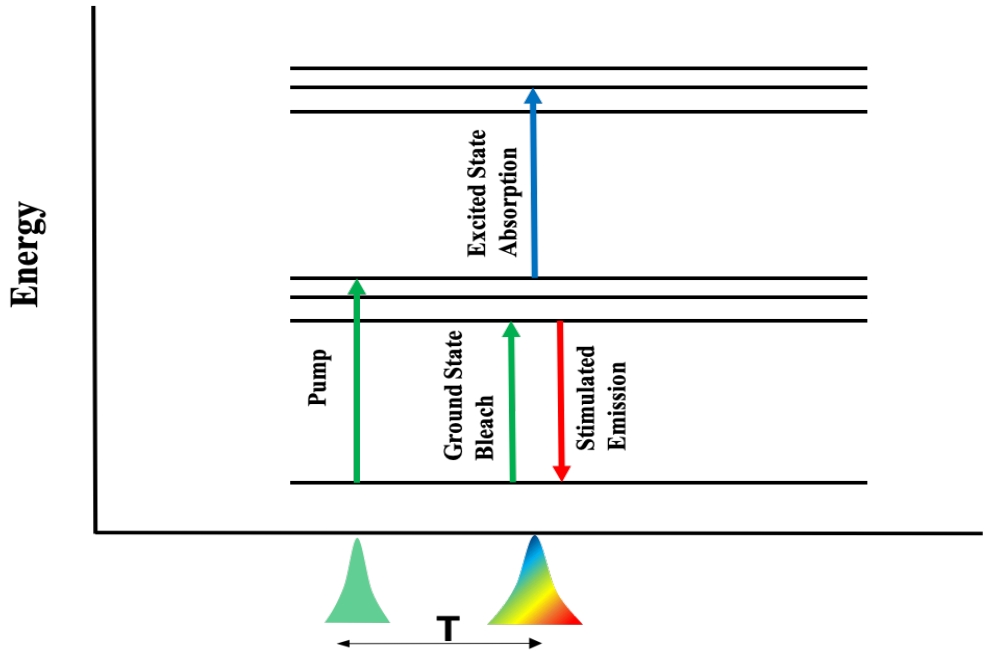

Figure 2.2: Energy level diagram for a hypothetical molecule

1. **Ground State Bleach (GSB):** When the pump pulse excites the sample, some part of the ground state population is transferred to the excited state resulting in depletion in the ground state population. Therefore, the absorption of the probe at wavelength of ground state absorption is decreased and thus a negative differential absorption (ΔA) is seen. This contribution to the signal is called as ground state bleach (GSB). With time, the excited state molecules return to the ground state and therefore the GSB signal decays and eventually come to zero.

2. **Stimulated Emission (SE):** When there is some population in the excited state, the photons in probe stimulate the emission of the molecules. These emitted photons have same direction, wavelength and polarization as the probe photons. When the pump is blocked, the number of photons reaching the detector is the total photons contained in the probe. When the pump is on, the number of photons reaching the

detector is the number of photons in the probe plus the photons emitted by the sample. Thus, $I_{pump\ on} > I_{pump\ off}$. Therefore, from equation (2.8) we will have a negative differential absorption (ΔA) signal. This signal is called as stimulated emission (SE).

3. **Excited State Absorption (ESA):** The molecule in its excited state can absorb a photon from the probe and go to a higher lying excited state. In this case Apump on > Apump off and we have a positive differential absorption (ΔA) signal. This signal is called as excited state absorption (ESA) or photo induced absorption (PIA).

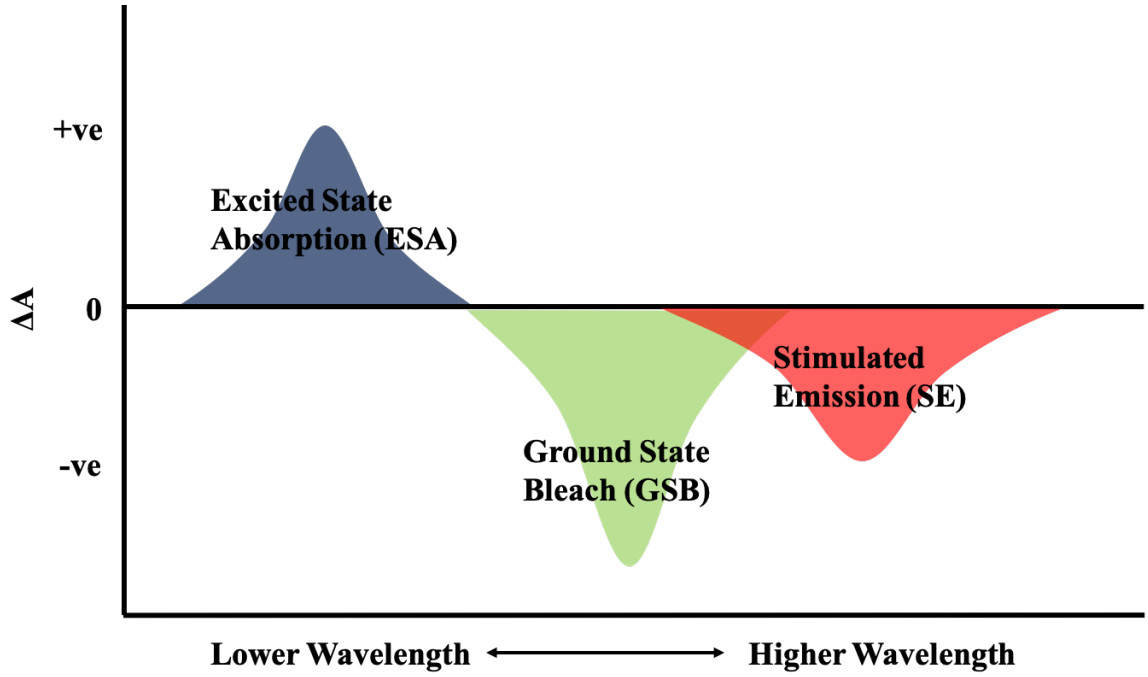

Figure 2.3: Types of signals in a pump – probe experiment

Two - Dimensional Electronic Spectroscopy

Two-dimensional electronic spectroscopy (2DES) is a third order non-linear spectroscopy which involves a four-wave mixing process. Three pulses with controllable interpulse delays interact with the sample and an emitted non-linear signal is detected [4].

2DES can be considered as an extension to a pump probe spectroscopy but it overcomes the shortcomings of a pump probe experiment. In a 2DES experiment, the overlapping responses can be separated by correlating the detection frequency with the excitation frequency.

In both pump probe and 2DES, the time resolution along the waiting time (i.e. the time between the pump and the probe pulse) is determined by the pulse width of the pump pulse (shorter the pulse width, higher is the time resolution). But shorter the temporal width of a pulse, larger is the bandwidth (as dictated by the Fourier transform relation) so resolution either in frequency or time domain is diminished [5].

The trade-off can be overcome using 2D Spectroscopy by employing the methods of Fourier transformation. The excitation axis is resolved by employing a pair of broadband pump pulses and scanning the delay between them. The signal generated oscillates as a function of delay between the two pump pulses (**τ**) and Fourier transformation along the **τ** axis helps one to obtain the excitation axis. Thus, one obtains high resolution in both temporal and spectral domains.

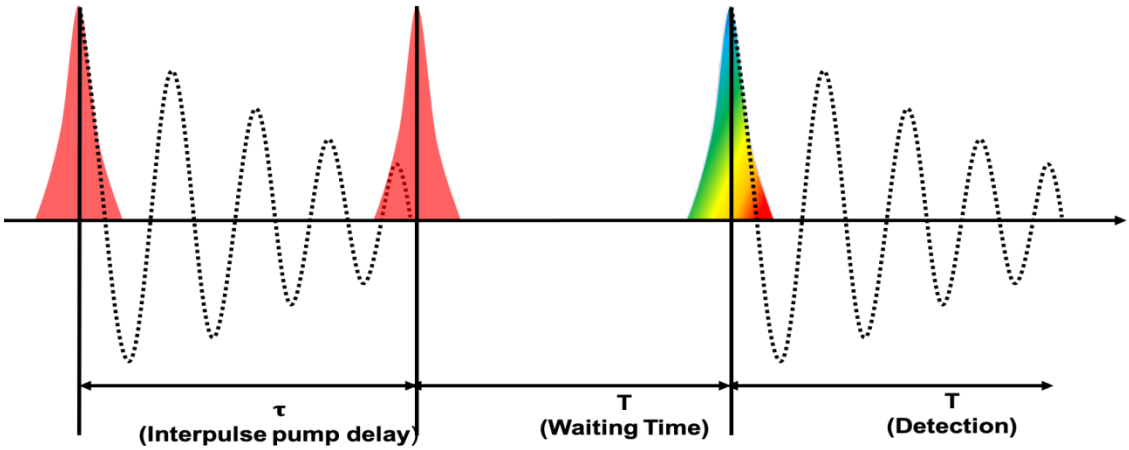

Figure 3.1: Pulse sequence for 2DES

In 2D FT, two different types of signals are generally collected based on the phase matching conditions: One being the rephasing and the other being the non-rephasing in the direction $-\mathbf{k_1}+\mathbf{k_2}+\mathbf{k_3}$ and $\mathbf{k_1}-\mathbf{k_2}+\mathbf{k_3}$ respectively. The direction of the rephasing and the non-rephasing signal is determined by the kind of geometry employed for the experiment [5]. The various kinds of geometries for a 2D-FT spectroscopy are:

1. **Fully collinear geometry:** All three pulses interact with the sample in a fully collinear geometry. The signal contains a lot of unwanted background which require extensive phase cycling schemes. Also, fluorescence is detected instead of stimulated signals, so is limited to fluorescing samples.

2. **Fully non-collinear boxcars geometry:** Three pulses at separate path interact with the sample. Maintaining the interpulse phase stability is a tedious task especially for shorter wavelengths. The direction of the rephasing an non-rephasing signal in boxcars geometry is shown in figure (3.2).

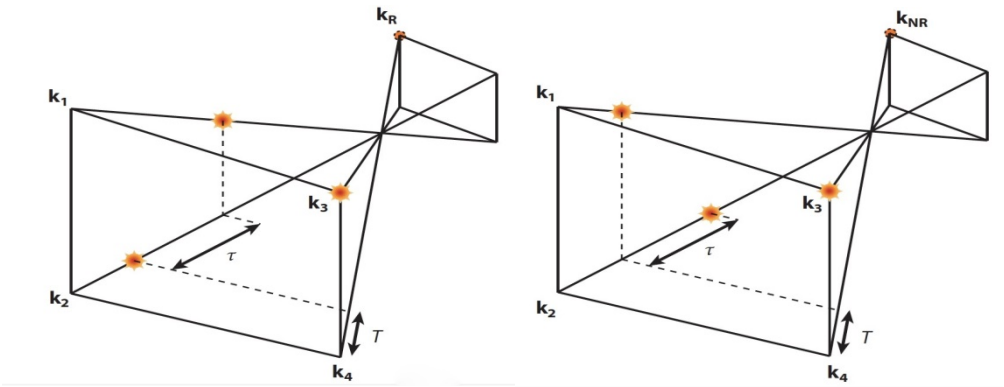

Figure 3.2: Direction for rephasing and non-rephasing signals in fully non-collinear boxcar geometry

3. **Partially non-collinear geometry (Pump – Probe based):** Two excitation pulses interact with the sample in a collinear fashion while a third pulse enters at a small angle w.r.t. to other two pulses. Two pulses with precise delay and relative phase can be generated using a pulse shaper. Few step phase cycling can completely retrieve the desired signal. The emitted third order signal is in the same direction as the third pulse which also removes the necessity of using a local oscillator for the heterodyned detection [4]. The direction of signal in a pump – probe based geometry is shown in figure (3.3).

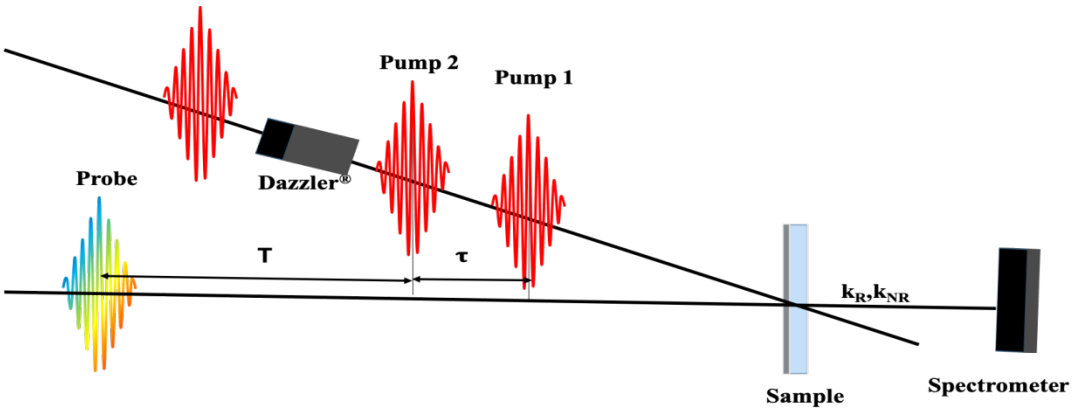

Figure 3.3: Direction for rephasing and non-rephasing signals in pump probe geometry

3.1. Theory

In pump-probe geometry, the electric field can be expressed as:

$$\begin{aligned}\mathbf{E(t) = A_1(t + T_w + \tau)\exp\left(-i\omega_L t + i\phi_{21} + i\Delta\omega_{ref}\tau + ik_{pump}r\right)}\\ \mathbf{+A_2(t + T_w)\exp\left(-i\omega_L t + ik_{pump}r\right)}\\ \mathbf{+A_3(t)\exp\left(-i\omega_L t + ik_{probe}r\right) + c.c.}\end{aligned} \quad \mathbf{(3.1)}$$

Where,

τ = delay between the two excitation pump pulses

$\phi_{21} = \phi_2 - \phi_1$ = relative phase between the two pump pulses

A_1 = pulse envelope of the first pump pulses

A_2 = pulse envelope of the second pump pulse

A_3 = pulse envelope of the probe pulse

ω_L = laser pulse center frequency

For a two-level system with energy gap of $\hbar\omega_{10}$, the third order non-linear response of a four-wave mixing experiment can be represented as:

$$\mathbf{R_R(\tau, t) = \Theta(\tau)\Theta(t)\exp(i\omega_{10}\tau)\exp(-i\omega_{10}t)F_R(\tau, t)} \quad \mathbf{(3.2)}$$

$$\mathbf{R_{NR}(\tau, t) = \Theta(\tau)\Theta(t)\exp(-i\omega_{10}\tau)\exp(-i\omega_{10}t)\,F_{NR}(\tau, t)} \quad \textbf{(3.3)}$$

R_R = rephasing response function; R_{NR} = non-rephasing response function

$\boldsymbol{\Theta}$ = Heaviside step function; ω_{10} = resonant frequency of the two – level system; F = peak shape function.

Assuming the interaction to be impulsive, the frequency resolved measurement after the spectrometer with a square law detector is:

$$\tilde{\mathbf{S}}(\emptyset_{21}; \tau, \omega_t) = \mathbf{Re}\left[\begin{matrix}\mathbf{F_R(\tau, \omega_t - \omega_{10})\exp(i\Delta\omega_{10}\tau)\exp(i\emptyset_{21})} \\ \mathbf{+F_{NR}(\tau, \omega_t - \omega_{10})\exp(-i\Delta\omega_{10}\tau)\exp(-i\emptyset_{21}) + P}\end{matrix}\right]$$

$$\begin{aligned} &= \mathbf{F_R(\tau, \omega_t - \omega_{10})\exp(i\Delta\omega_{10}\tau)\exp(i\emptyset_{21})} \\ &+ \mathbf{F_{NR}(\tau, \omega_t - \omega_{10})\exp(-i\Delta\omega_{10}\tau)\exp(-i\emptyset_{21})} \\ &+ \mathbf{F_R^*(\tau, \omega_t - \omega_{10})\exp(-i\Delta\omega_{10}\tau)\exp(-i\emptyset_{21})} \\ &+ \mathbf{F_{NR}^*(\tau, \omega_t - \omega_{10})\exp(i\Delta\omega_{10}\tau)\exp(i\emptyset_{21}) + P} \end{aligned} \quad \textbf{(3.4)}$$

$\Delta\omega_{10} = \omega_{10} - \omega_{ref}$ = resonance frequency detuned from the reference frequency ω_{ref}

$F_R(\tau, \omega_t - \omega_{10})$ = Fourier transform of $F_R(\tau, t)$ about t

$F_{NR}(\tau, \omega_t - \omega_{10})$ = Fourier transform of $F_{NR}(\tau, t)$ about t

P = Phase ($\emptyset_{21}$) independent terms i.e. pump probe from individual pulses and linear absorption signals

3.2. Data Processing

According to causality condition, there should be no signal before t = 0. Data is first inverse Fourier transformed with respect to ω_t in equation (3.4):

$$\begin{aligned} \tilde{\mathbf{S}}(\emptyset_{21}; \tau, t) = \ & \mathbf{\Theta(\tau)\Theta(t)\exp(i\Delta\omega_{10}\tau)\exp(-i\omega_{10}t)\exp(i\emptyset_{21})\,F_R(\tau, t)} \\ & \mathbf{+\Theta(\tau)\Theta(-t)\exp(-i\Delta\omega_{10}\tau)\exp(-i\omega_{10}t)\exp(-i\emptyset_{21})\,F_R^*(\tau, -t)} \\ & \mathbf{+\Theta(\tau)\Theta(t)\exp(-i\Delta\omega_{10}\tau)\exp(-i\omega_{10}t)\exp(-i\emptyset_{21})\,F_{NR}(\tau, t)} \\ & \mathbf{+\Theta(\tau)\Theta(-t)\exp(i\Delta\omega_{10}\tau)\exp(-i\omega_{10}t)\exp(i\emptyset_{21})\,F_{NR}^*(\tau, -t) + \tilde{P}} \end{aligned} \quad \textbf{(3.5)}$$

Therefore, the terms with $\Theta(-t)$ are discarded and equation (3.5) is then Fourier transformed along t to give:

$$\tilde{S}'(\emptyset_{21};\tau,\omega_t) = \begin{matrix} F_R(\tau,\omega_t - \omega_{10})\exp(i\Delta\omega_{10}\tau)\exp(i\emptyset_{21}) \\ +F_{NR}(\tau,\omega_t - \omega_{10})\exp(-i\Delta\omega_{10}\tau)\exp(-i\emptyset_{21}) + P \end{matrix} \quad (3.6)$$

The relevant 2D spectra from equation (3.6) can only be obtained after employing the method of phase cycling.

3.3. Theory of Phase Cycling [6]:

- Phase of all but one pulse is varied in increments of $2\pi/l_i(0, 2\pi/li\ , 2\times 2\pi/li\ \ldots)$.
- Here $L = l_1 \times l_2 \times \ldots$ is called as L step phase cycling.
- The total signal is multiplied by complex conjugate of the particular signal phase.
- The signal from desired pathway gets a weight of 1 while weight from unwanted pathways is different.
- This process is then repeated and the resulting signals are then added so that the desired signal gets a weightage equal to total phase combinations and unwanted signal gets a weight of zero.

3.3.1. Two –step phase cycling scheme

In a two–step phase cycling scheme, the interpulse phases between the two pump pulses is cycled between 0 and π and the data is then processed as follows [4]:

$$\tilde{S}(\emptyset_{21};\tau,\omega_t) = \begin{matrix} F_R(\tau,\omega_t - \omega_{10})\exp(i\Delta\omega_{10}\tau)\exp(i\emptyset_{21}) \\ +F_{NR}(\tau,\omega_t - \omega_{10})\exp(-i\Delta\omega_{10}\tau)\exp(-i\emptyset_{21}) + P \end{matrix} \quad (3.7)$$

For $\Delta\emptyset_{21} = 0$;

$$\tilde{S}(\emptyset_{21};\tau,\omega_t) = F_R(\tau,\omega_t - \omega_{10})\exp(i\Delta\omega_{10}\tau)\exp(i\Delta\emptyset_{21})\,exp(-i0)$$
$$+F_{NR}(\tau,\omega_t - \omega_{10})\exp(-i\Delta\omega_{10}\tau)\exp(-i\Delta\emptyset_{21})\,exp(-i0) + P\,exp(-i0)$$

$$= F_R(\tau,\omega_t - \omega_{10})\exp(i\Delta\omega_{10}\tau) + F_{NR}(\tau,\omega_t - \omega_{10})\exp(-i\Delta\omega_{10}\tau) + P \quad (3.8)$$

For $\Delta\emptyset_{21}$=π;

$$\tilde{S}(\Delta\emptyset_{21};\tau,\omega_t) = F_R(\tau,\omega_t - \omega_{10})\exp(i\Delta\omega_{10}\tau)\exp(i\Delta\varphi_{21})\exp(-i\pi)$$
$$+ \quad F_{NR}(\tau,\omega_t - \omega_{10})\exp(-i\Delta\omega_{10}\tau)\exp(-i\Delta\varphi_{21})\exp(-i\pi) + P\exp(-i\pi)$$

$$= \mathbf{F_R(\tau, \omega_t - \omega_{10})\exp(i\Delta\omega_{10}\tau) + F_{NR}(\tau, \omega_t - \omega_{10})\exp(-i\Delta\omega_{10}\tau) - P} \quad \textbf{(3.9)}$$

Adding equation (3.8) and equation (3.9), we get

$$\mathbf{S_{total} = 2F_R(\tau, \omega_t - \omega_{10})\exp(i\Delta\omega_{10}\tau) + 2F_{NR}(\tau, \omega_t - \omega_{10})\exp(-i\Delta\omega_{10}\tau)}$$

Fourier transformation along $\boldsymbol{\tau}$:

$$\mathbf{S_{total} = 2F_R(\omega_\tau + \Delta\omega_{10}, \omega_t - \omega_{10}) + (\omega_\tau - \Delta\omega_{10}, \omega_t - \omega_{10})} \quad \textbf{(3.10)}$$

Although, 2 step phase cycling scheme can help to remove phase independent terms, it cannot separate the rephasing signal and the non-rephasing signal. This can be done using a three-step phase cycling scheme.

3.3.2. Three – step phase cycling scheme

In a three–step phase cycling scheme, the interpulse phases between the two pump pulses is cycled between 0, $\frac{2\pi}{3}$ and $\frac{4\pi}{3}$ and the data is then processed in a similar way as done for a two-step phase cycling scheme [4].

To obtain the rephasing signal, the signal at each inter pump pulse phase ($\Delta\emptyset_{21}$) is multiplied by $-\mathbf{i}(\Delta\emptyset_{21})$ and all these signals are added as follows:

$$\mathbf{S_{rephasing} \propto 1 \times S}(\Delta\emptyset_{21} = 0) + \exp\left(-\frac{i2\pi}{3}\right) \times \mathbf{S}\left(\Delta\emptyset_{21} = \frac{2\pi}{3}\right) + \exp\left(-\frac{i4\pi}{3}\right) \times \mathbf{S}\left(\Delta\emptyset_{21} = \frac{4\pi}{3}\right) \quad \textbf{(3.11)}$$

Total Weight = 3

$$\mathbf{S_{non-rephasing} \propto 1 \times S}(\Delta\emptyset_{21} = 0) + \exp\left(-\frac{i2\pi}{3}\right) \times \mathbf{S}\left(\Delta\emptyset_{21} = \frac{2\pi}{3}\right) + \exp\left(-\frac{i4\pi}{3}\right) \times \mathbf{S}\left(\Delta\emptyset_{21} = \frac{4\pi}{3}\right) \quad \textbf{(3.12)}$$

Total Weight = 0

To obtain the non-rephasing signal, the signal at each inter pump pulse phase ($\Delta\varphi_{21}$) is multiplied by $\mathbf{i}(\Delta\emptyset_{21})$ and all these signals are added as follows:

$$\mathbf{S_{rephasing} \propto 1 \times S(\Delta\emptyset_{21} = 0) + exp\left(\frac{i2\pi}{3}\right) \times S\left(\Delta\emptyset_{21} = \frac{2\pi}{3}\right) + exp\left(\frac{i4\pi}{3}\right) \times S\left(\Delta\varphi_{12} = \frac{4\pi}{3}\right)} \quad \textbf{(3.13)}$$

Total Weight = 0

$$\mathbf{S_{non-rephasing} \propto 1 \times S(\Delta\emptyset_{21} = 0) + exp\left(\frac{i2\pi}{3}\right) \times S\left(\Delta\emptyset_{21} = \frac{2\pi}{3}\right) + exp\left(\frac{i4\pi}{3}\right) \times S\left(\Delta\emptyset_{21} = \frac{4\pi}{3}\right)} \quad \textbf{(3.14)}$$

Total Weight = 3

From equation (3.11) – (3.14), it can be seen that using a three-step phase cycling the phase independent signals can be removed and also the rephasing and non – rephasing components can be separated.

3.4. Rephasing and Non-rephasing Signals [7]

After the interaction with the first pulse, the Bloch vectors of individual molecules start to oscillate with their frequencies and run out of phase with time. During the period t_1, the faster molecules lead and slower will lag behind. After the interaction with the second and the third pulse, each of the Bloch vectors are mirrored on B_y axis and the molecules which were lagging will now be in front of others. They tend to rotate slower during the time t_3 such the individual vectors rephase at time $t_1 = t_3$. This reappearance of macroscopic polarization is known as photon echo (similar to spin echo in NMR) and occurs whenever there is inhomogeneous broadening. This pulse sequence is called as photon echo or rephasing pulse sequence and corresponding signal is called a rephasing signal.

On the other hand, if the Bloch vectors continue to rotate unchanged during t_3, it is called a non-rephasing signal.

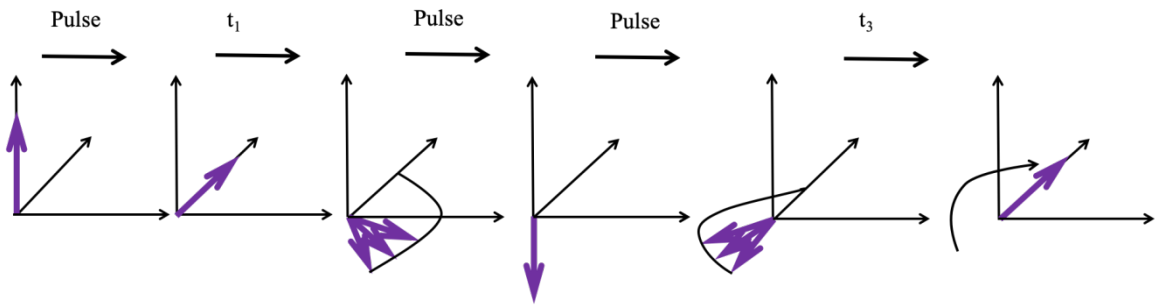

Figure 3.4: Photon-echo (rephasing) pulse sequence

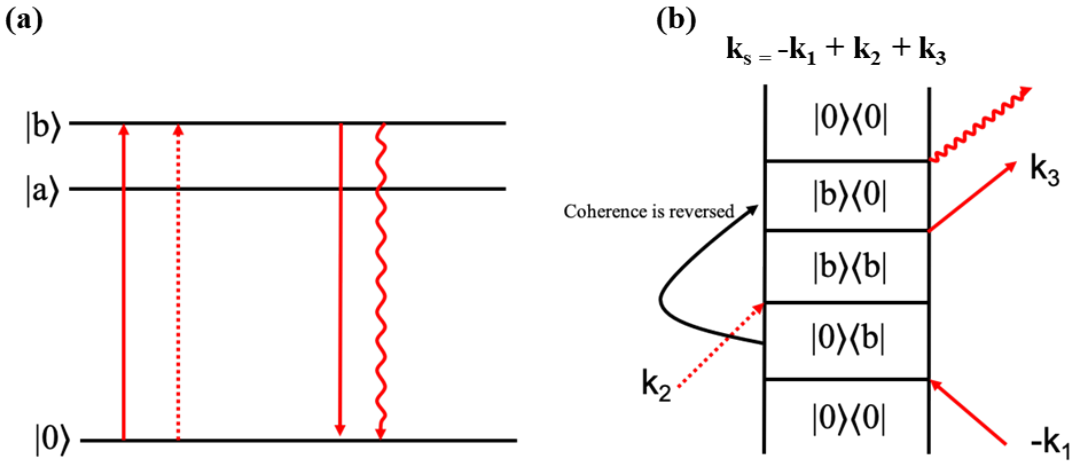

Figure 3.5: (a) Energy level diagram & (b) double sided Feynman diagram for a rephasing signal

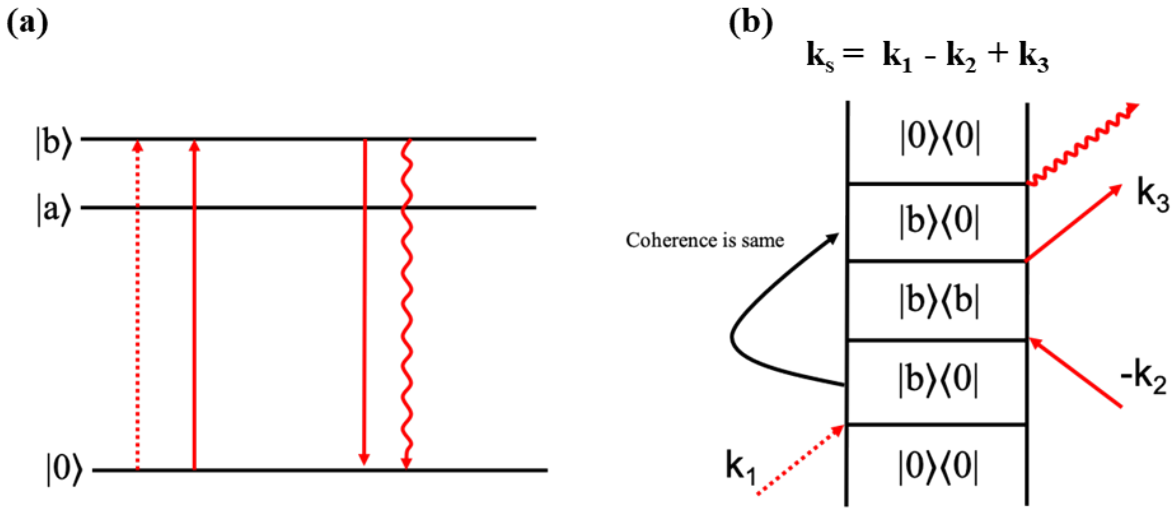

Figure 3.6: Energy level diagram and double-sided Feynman diagram for a non-rephasing signal

3.5. Complete route to post processing the data

The complete route to processing the data after the collection of data using a three-step phase cycling scheme is summarized in figure (3.7) [4].

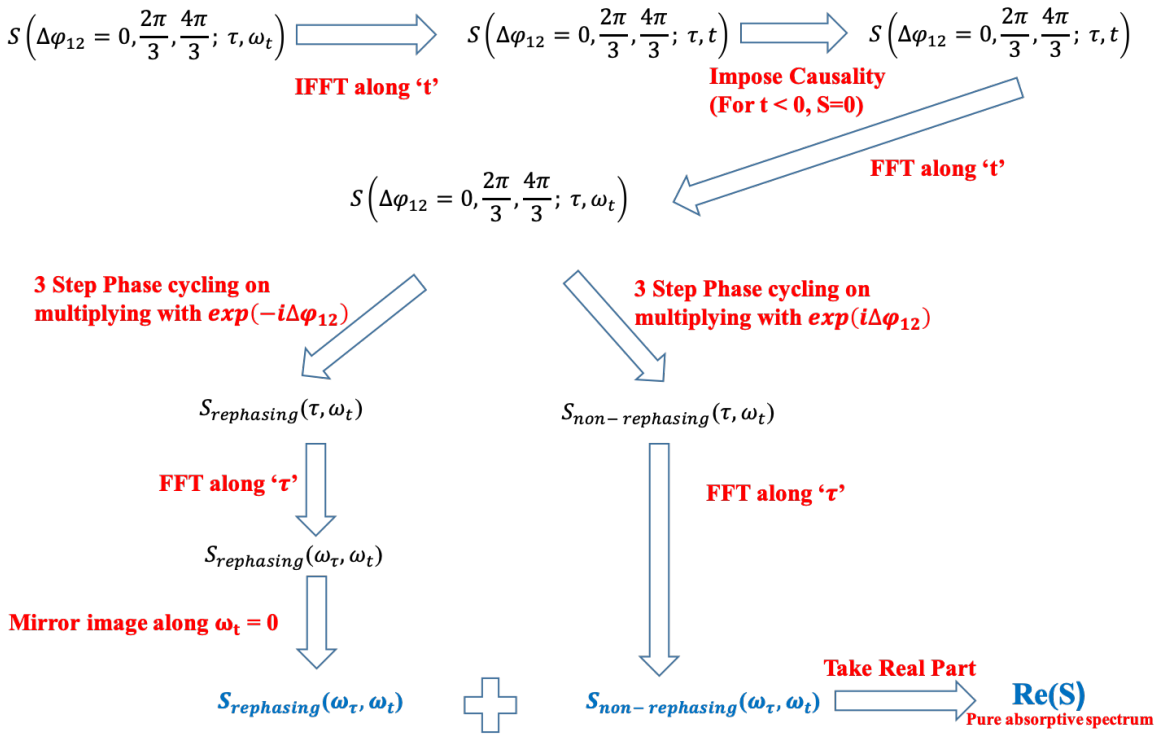

Figure 3.7: Complete route to process the data using a three-step phase cycling scheme

Polar Solvation Dynamics

4. Study of Polar Solvation using TAS

5. Study of Polar Solvation using 2DES

Study of Polar Solvation using TAS

4.1. Introduction

Emission from a chromophore usually occurs at the wavelengths that are red shifted with respect to the absorption wavelengths. Initially the chromophore is excited to higher vibrational states of the first singlet state (S_1). This vibrational energy is then lost to solvent and the chromophore comes to the lowest vibrational state of the excited state from which emission. The chromophore may also be excited to higher electronic state (S_n) which then relaxes to S_1 (known as internal conversion) from which emission occurs. Both these processes result in the red shift (Stokes shift) of the emission spectrum [8].

A polar solvent can stabilize the excited state and the emission can then be shifted to still longer wavelengths (lower energy). Fluorophores have larger dipole moment in the excited state (μ_E) than in the ground state (μ_G). After the excitation the solvent dipoles can reorient themselves around the fluorophore dipole which can then lower the energy of the excited state. With increase in polarity of the solvent, the effect becomes more prominent and emission takes place at much longer wavelengths from the relaxed states. Polar molecules are much sensitive to the solvent environment as compared to non-polar molecules. The spectral shift is related to the solvent correlation function by following equation [8]:

$$\mathbf{C(t)} = \frac{\mathbf{\upsilon(t)-\upsilon(0)}}{\mathbf{\upsilon(0)-\upsilon(\infty)}} \qquad \textbf{(4.1)}$$

where, $\nu(0)$, $\nu(t)$ and $\nu(\infty)$ are the central frequencies corresponding to Stokes shift at the time '0', 't' and 'infinity' respectively.

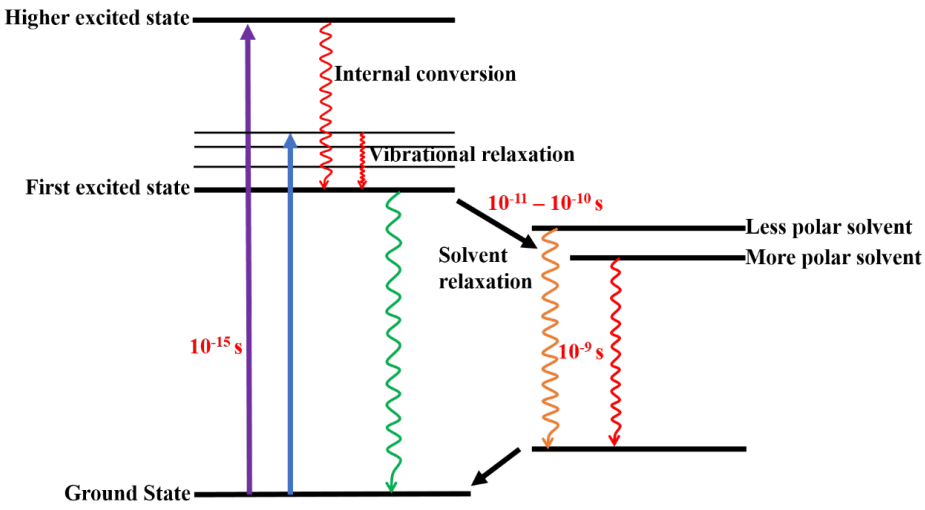

Figure 4.1: Jablonski diagram showing the effect of solvent polarity

The chromophore can emit before or during the relaxation by the solvent and the emission spectra will then display time dependent changes. Such effects are not seen in steady state spectra and can only be seen in time- resolved measurements such as the intensity decays at various wavelengths. The nature of intensity decays depends on the detection wavelength.

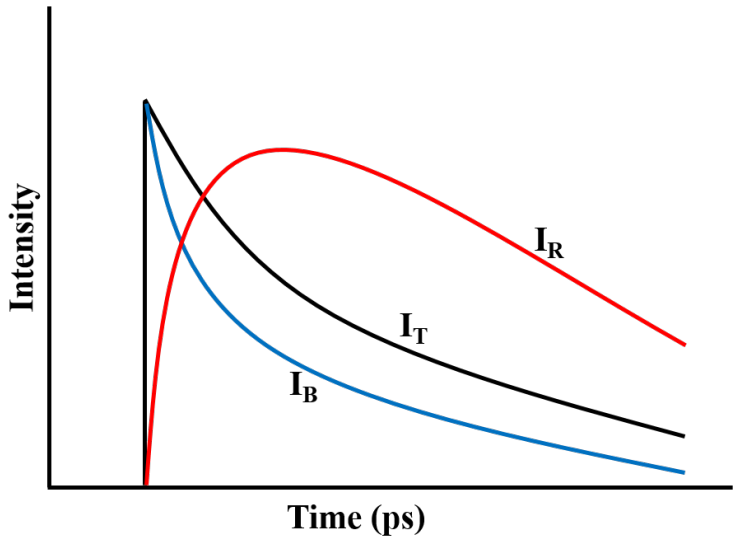

Figure 4.2: Intensity decays for different wavelengths

In figure (4.2), I_T, I_B and I_R are the total fluorescence intensity decay, decay at blue wavelength and decay at red wavelength respectively. The intensity for blue wavelength decays faster than the total decay because it decays both by emission as well as relaxation

while the intensity for red wavelength first rises because of the time required for relaxation from blue to red wavelength as well as the decay is slower.

4.2. Results and discussion

The dynamics of two different solvents (ethanol and ethylene glycol) are studied using DNTTCI as a probe and the correlation function are made from the spectrally resolved femtosecond pump probe data.

4.2.1. Steady state analysis

DNTTCI dye was chosen since the laser spectrum covers only red edge of the absorption and most of the emission spectrum such that the contribution from vibrational relaxation is less. The overlap of absorption and emission of the dye with the laser spectrum is shown in figure (4.3).

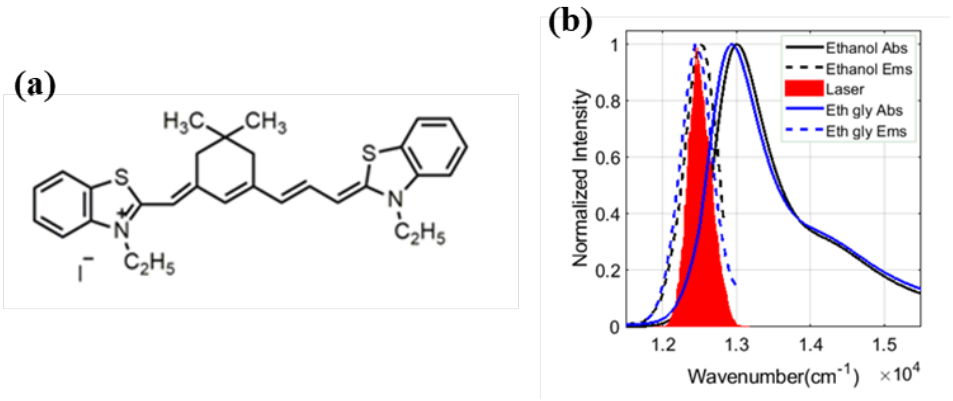

Figure 4.3: (a) Molecular structure of DNTTCI dye & (b) overlap of laser spectrum with absorption and emission spectrum of DNTTCI

The change is dipole moment upon photo-excitation is given by Lippert's equation [8]:

$$\Delta\bar{\nu} = \bar{\nu}_A - \bar{\nu}_F = \frac{2}{hc}\left[\frac{\epsilon-1}{2\epsilon+1} - \frac{\eta^2-1}{2\eta^2+1}\right]\frac{(\mu_E-\mu_G)^2}{a^3} \qquad (4.2)$$

Where $\bar{\nu}_A$ and $\bar{\nu}_F$ are the absorption and emission frequencies (cm^{-1}), a is the radius of the solute molecule, ϵ is dielectric constant and η the refractive index of the solvent. The ratio of change in dipole moment of DNTTCI in ethylene glycol and ethanol is $\frac{(\Delta\mu)_{Eth\ Gly}}{s(\Delta\mu)_{Ethanol}} =$

1.03, so, the initial charge redistribution in the two solvents is similar and the difference in the dynamics due to the nature of the solvent alone.

4.2.2. Pump probe analysis

A 1 kHz repetition rate amplified Ti: Sapphire system (Libra, Coherent) was used as the laser source with a central wavelength at ~ 800 nm and pulse width ~55 fs.
Beam splitters were used to split the 800 nm beam into the pump and the probe. The pump and probe were routed to femtosecond transient absorption spectrometer and were overlapped inside the sample. The delay between the pump and the probe was controlled using a mechanical delay stage (ILS300LM, Newport Corp.) which can provide a delay of up to 4 ns with a minimum step size of ~0.13 fs. A mechanical chopper (New Focus 3502) running at a repetition of 500 Hz was used which blocks every alternate pump pulse to generate differential absorption signal ($\Delta OD/\Delta A$) at each pump – probe delay. The transmitted probe was sent then sent to a spectrometer.

Using pump probe spectroscopy both vibrational relaxation as well as the solvation can be probed where a negative differential absorption (ΔOD) indicates the presence of a stimulated emission signal. In case of DNTTCI, the stimulated emission signal is red shifted (depending on the nature of the solvent) with increase in delay between the pump and the probe. In case of ethylene glycol due to presence of H-bonding network as well as higher viscosity, the dynamics are much slower. Figure (4.4) shows the spectral and time traces in the two solvents.

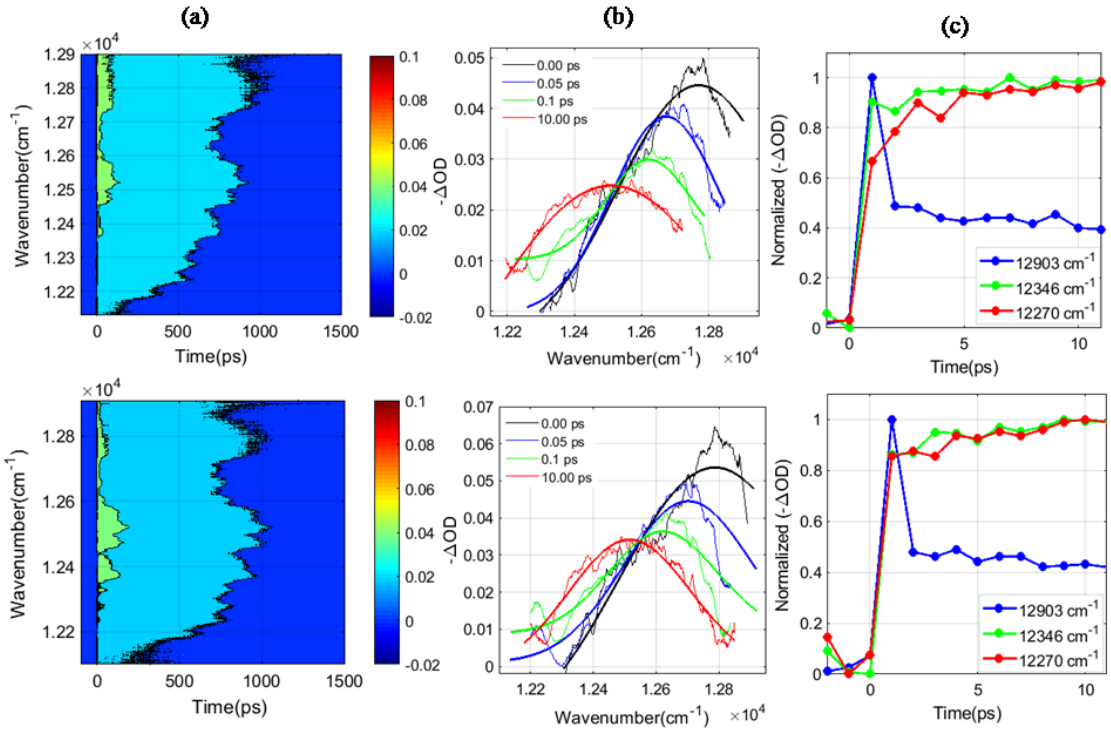

Figure 4.4: Plots for (a) pump – probe contour as a function of delay and wavelength, (b) spectral traces at different delays, and (c) time traces at different frequencies. Top: in ethanol, Bottom: in ethylene glycol

Pump – probe spectral traces for DNTTCI were fitted with lognormal from which the central frequencies at various time delays $\upsilon(t)$ were obtained. It is observed that the fully relaxed spectrum completely matches with the steady state spectrum $\upsilon(\infty)$. The correlation function was then constructed using equation (4.1). The shift in emission frequencies with time in ethanol and ethylene glycol and the corresponding correlation function are shown in figure (4.5).

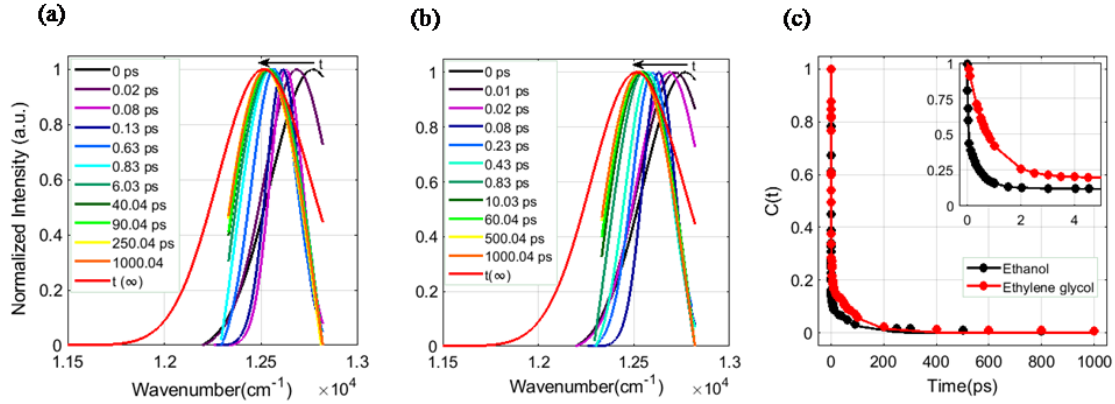

Figure 4.5: lots of spectral traces fitted to lognormal for (a) ethanol, (b) ethylene glycol and (c) correlation function

The parameters of the tri-exponential and bi-exponential fits of the correlation function are shown in table (1):

Parameters	α_2	τ_2(ps)	α_3	τ_3(ps)	R^2
Ethanol	0.769	0.460	0.252	63.09	0.998
Ethylene Glycol	0.737	0.780	0.275	68.92	0.962

Table 4.1: Parameters for the fit of correlation function for DNTTCI in ethanol and ethylene glycol.

From table (4.1), it can be seen the other two-time scales of 460 fs and 63 ps are faster in ethanol as than ethylene glycol which corresponds to the librational and translational motion.

Conclusion

Solvation correlation function can be constructed using spectrally resolved femtosecond pump – probe spectroscopy. Ultrafast solvation dynamics of ethanol and ethylene glycol have been studied and found that the there is significant different in the dynamics of the two solvents within 1 ps timescale. Also, the dynamics for both the solvents are over within 100 ps which are much less than the fluorescence lifetime of DNTTCI.

Study of Polar Solvation using 2DES

5.1. Introduction

2DES has been developed to study a number of condensed phase phenomena in sub – ps timescales. Using the technique of 2DES, correlation maps between excitation and emission frequencies can be drawn which are very helpful in resolving the overlapping molecular responses. Here the dynamics of ethanol using two dye probes (IR140 and DNTTCI) are studied using 2DES. Using the correlation maps of 2DES, excitation wavelength dependent solvation correlation function can be constructed to understand the dynamics of the solvent.

The 2DES setup is based on pump-probe geometry where the output of an amplified Ti: Sapphire (Coherent, Libra) system is used as both pump and probe pulses. The amplifier output is centered on 800nm (12,500cm^{-1}) with pulse width of ~55fs. A pulse shaper (Dazzler®, Fastlite) is integrated with a transient absorption spectrometer which helps to provide the two excitation pump pulses with controllable delay and phase [9].

5.2. Results and discussion

5.2.1. IR140

5.2.1.1.Steady state analysis

For IR140, the laser spectrum overlaps with maximum of the absorption but can probe only the blue edge of the emission spectrum. The overlap of the laser spectrum with absorption and emission of the dye is shown in figure (5.1).

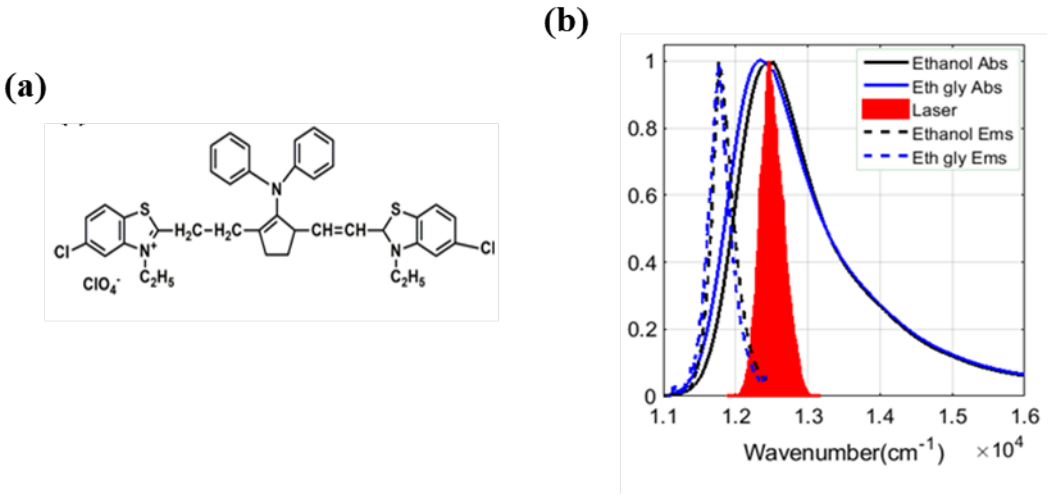

Figure 5.1: (a) Molecular structure of IR140 dye & (b) overlap of laser spectrum with absorption and emission spectrum of IR140

5.2.1.2. 2DES analysis

The data were collected using a 2-step phase cycling scheme where the delay between the two excitation pump pulses was scanned from -250fs to 0fs. The time zero corresponds to the temporal overlap of second pump and the probe pulse.

The signal was collected in time domain along the excitation axis which was later Fourier transformed (after imposing causality) using MATLAB®.

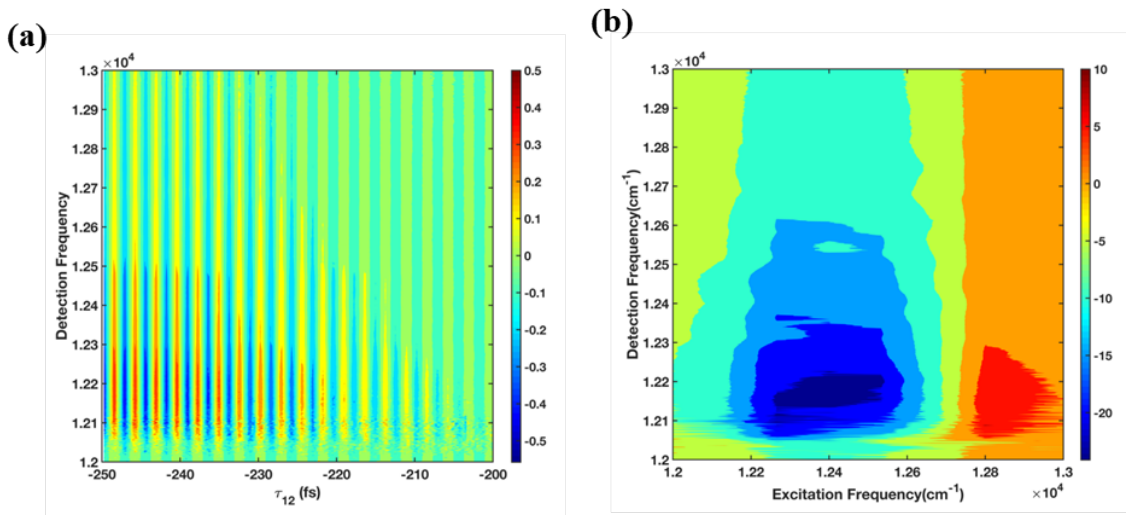

Figure 5.2: 2D spectra for a 2-step phase cycling scheme in (a) time domain & (b) real part of corresponding Fourier transformed spectra

To understand the significance of phase cycling, a slice at 12,500 cm^{-1} along detection axis is taken as shown in figure (5.3).

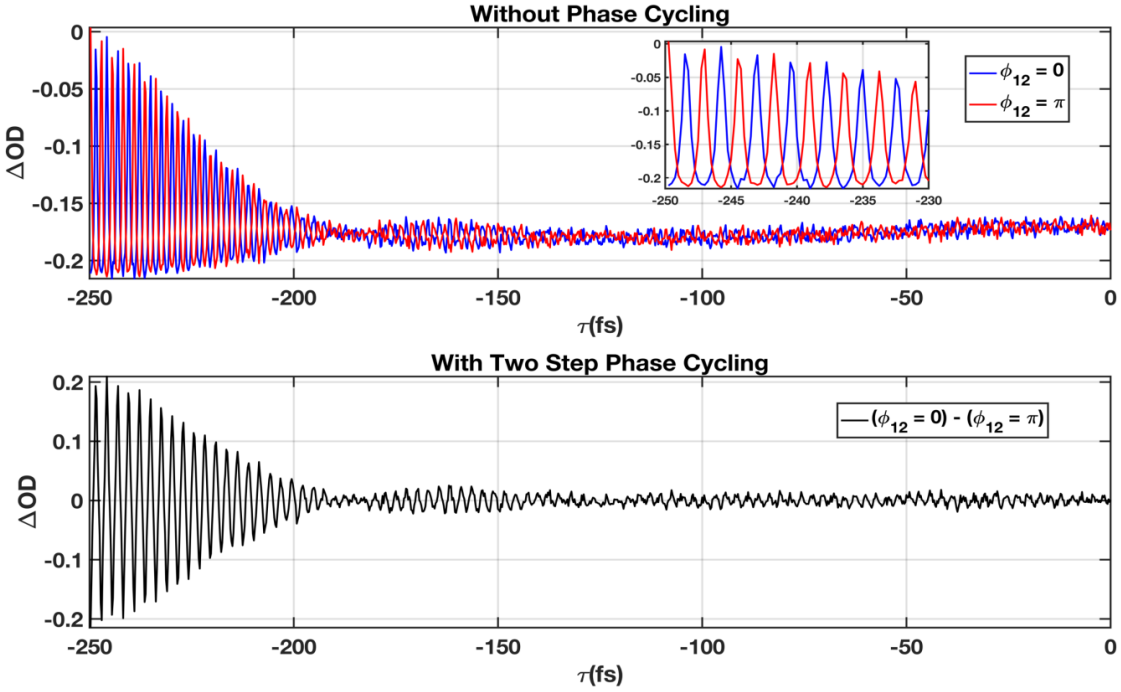

Figure 5.3: Slice at 12,500 cm^{-1} along detection axis for a two – step phase cycling. X-axis corresponds to the delay between the excitation pulses

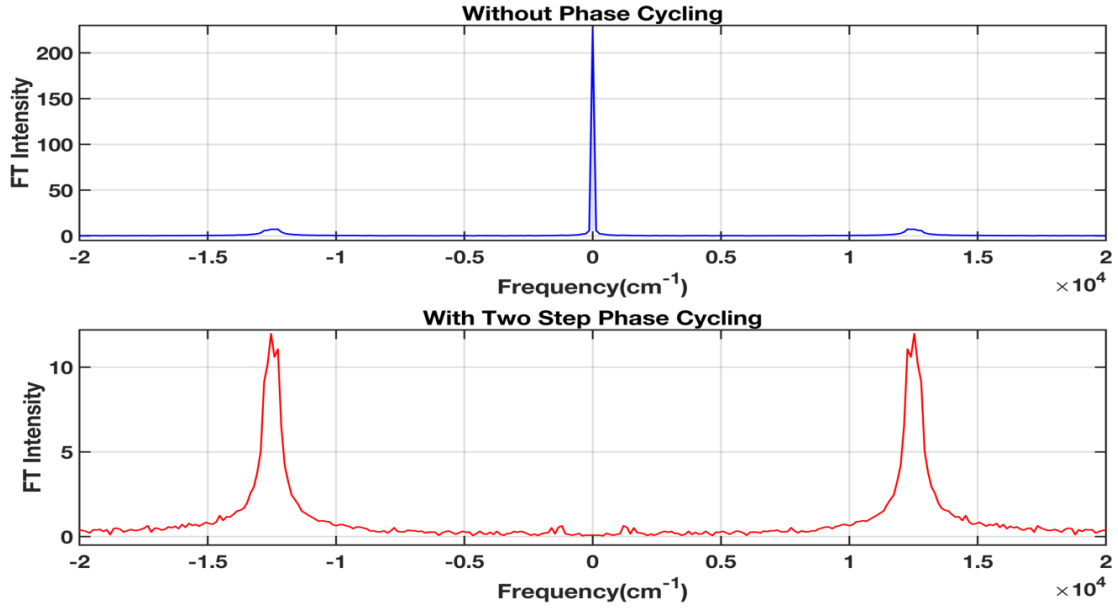

Figure 5.4: Fourier transformed spectra at a detection frequency of 12,500 cm^{-1}

From the Fourier transformed spectra it can be clearly seen that when no phase cycling scheme is employed, zero frequency background clearly dominates the signal while the required third order signal is overshadowed by this background signal. On using a 2-Step phase cycling scheme, the zero-frequency component is removed and the third order signal can now be clearly seen.

The real part of Fourier transformation gives the purely absorptive spectrum which is shown in figure (5.5) while the imaginary part gives the dispersion component [10] which is shown in figure (5.6).

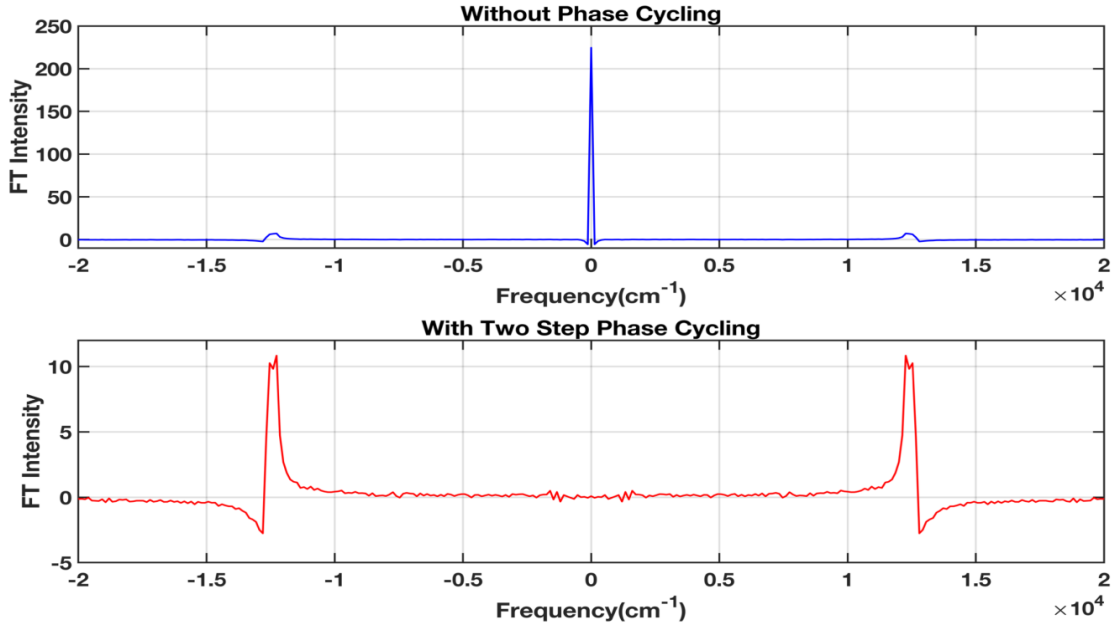

Figure 5.5: Real part of Fourier transformation of 2DES signal

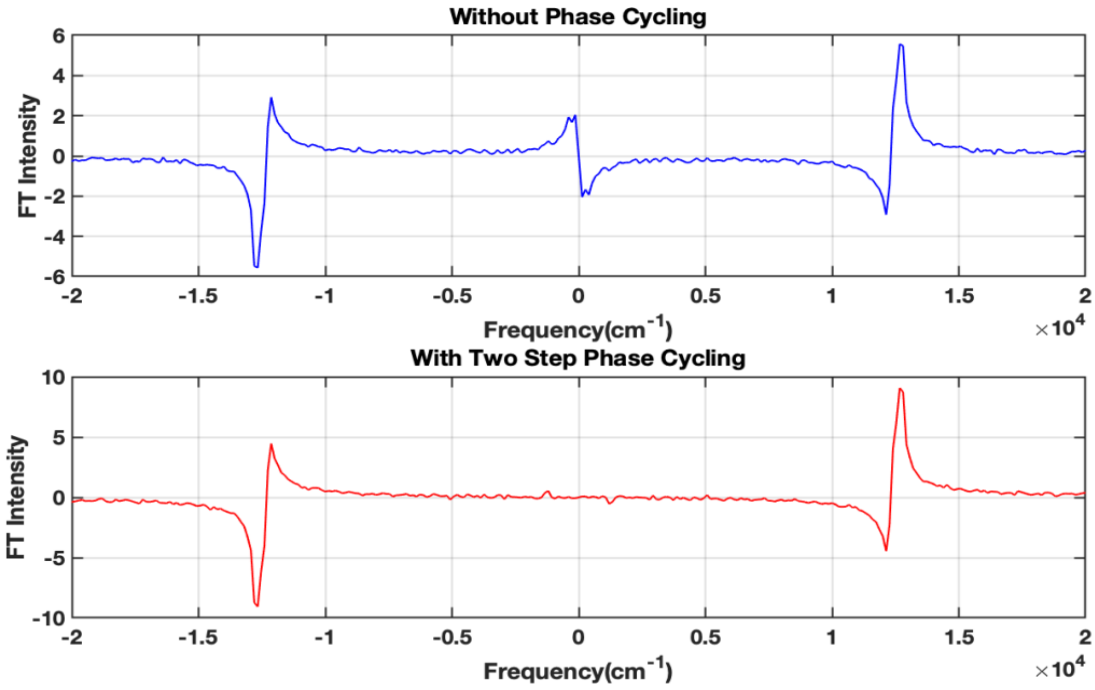

Figure 5.6: Imaginary part of Fourier transformation of 2DES signal

The data were collected at different waiting time i.e. the time between the second pump and the probe pulses and are shown in figure (5.7).

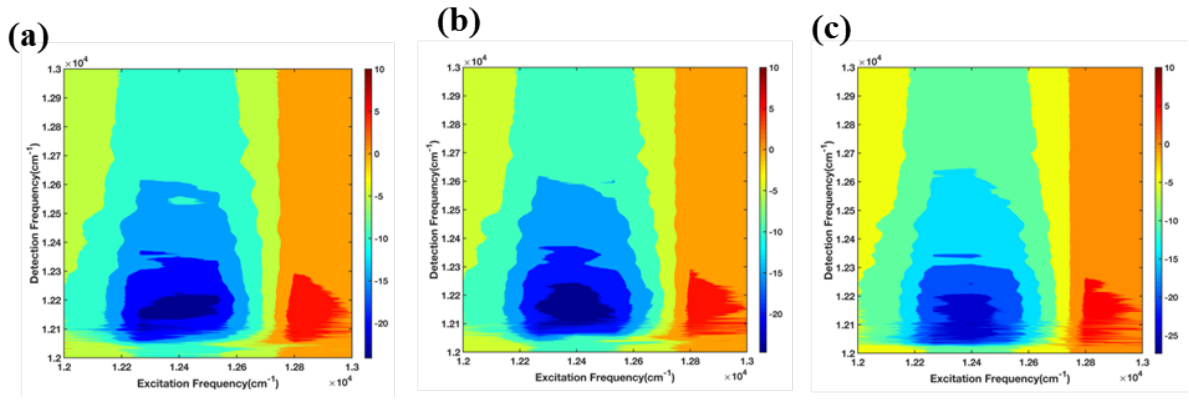

Figure 5.7: 2DES plots for IR-140 at (a) 0 ps (b) 0.1 ps & (c)1 ps using 2 – step phase cycling

Using a 2-step phase cycling scheme, the rephasing and non-rephasing signals cannot be separated. Therefore, a 3-step phase cycling scheme is required to separate the rephasing and the non-rephasing [4].

The time domain data at a detection frequency of 12,500 cm^{-1} using a three-step phase cycling is shown in figure (5.8).

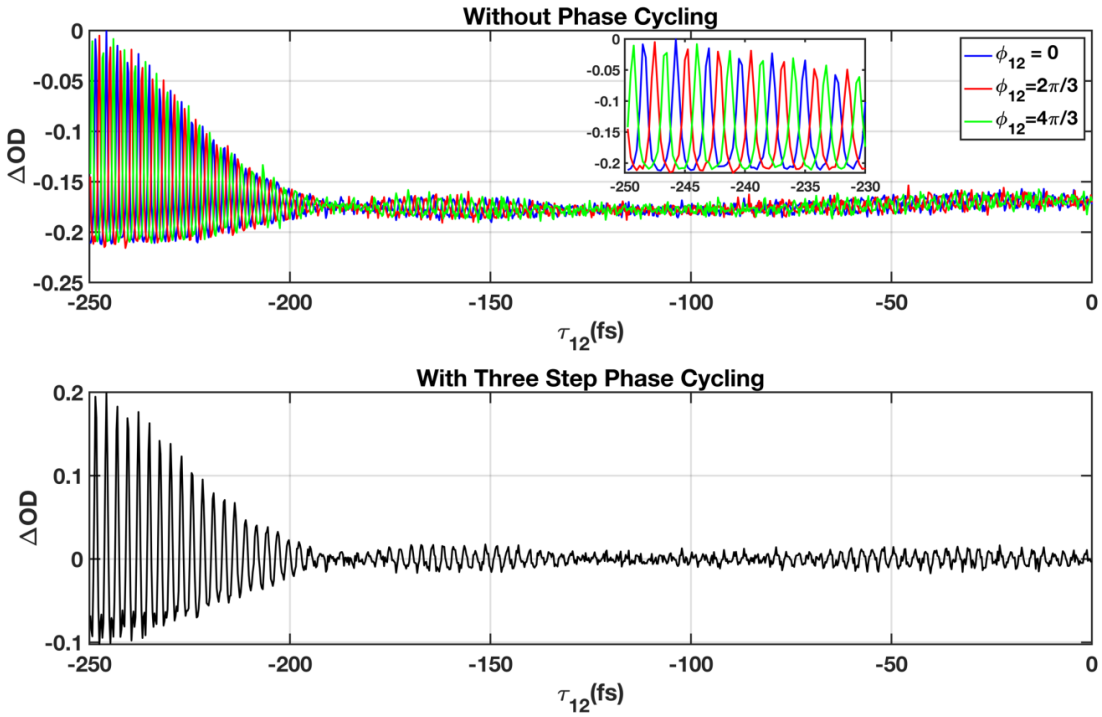

Figure 5.8: Slice at 12,500 cm^{-1} along detection axis. X-axis corresponds to the delay between the excitation pulses

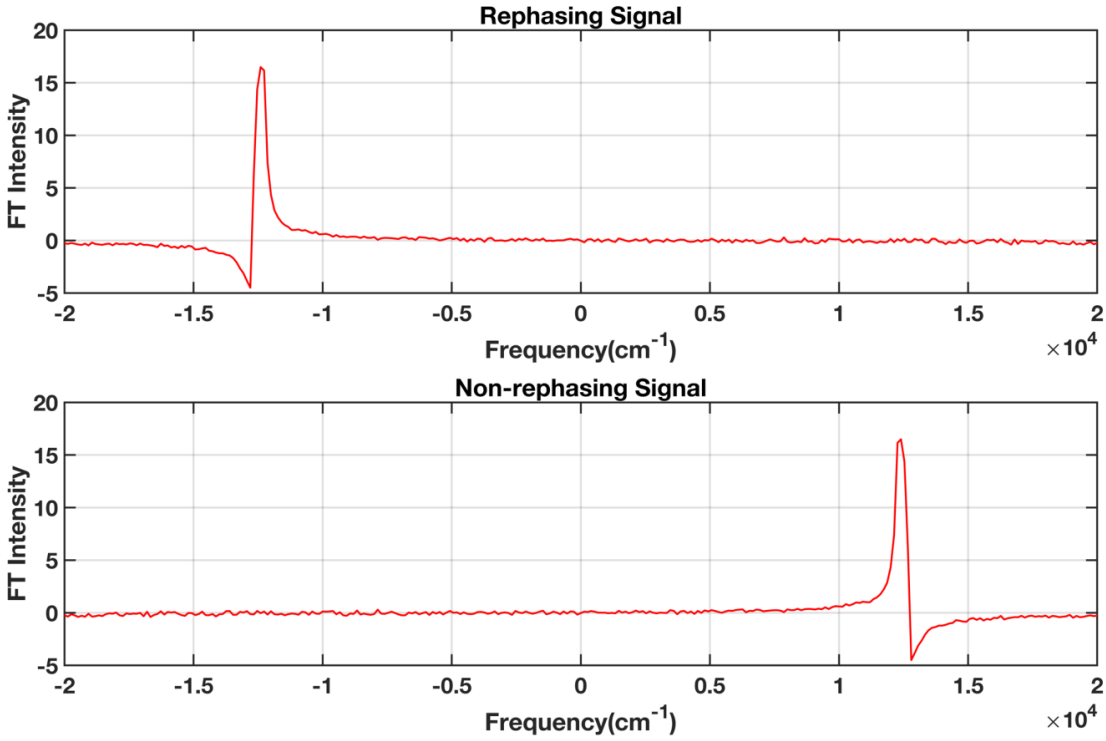

Figure 5.9: Real part of Fourier transformation showing the rephasing and the non-rephasing signal

From the figure (5.9), it is clearly seen that the rephasing and non-rephasing signals can be separated using a 3 –step phase cycling scheme. Also, the mirror image discrepancy seen in a 2 – step phase cycling is removed.

The purely absorptive spectrum is obtained after taking the mirror of real part of rephasing signal along positive frequency axis and adding it to the real part of non-rephasing signal. The three different types of signals are shown in figure (5.10).

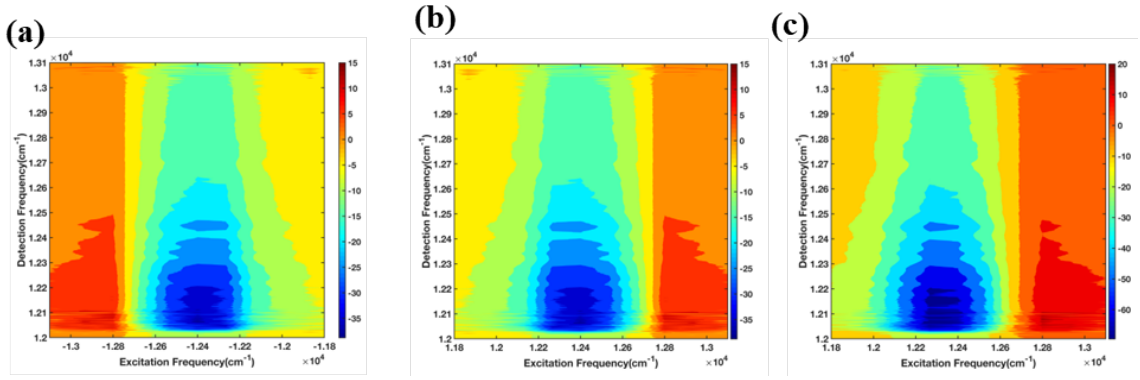

Figure 5.10: 2DES plots for IR-140 using 3-step phase cycling at 0ps for (a) rephasing signal (b) non-rephasing signal & (c) total purely absorptive spectrum

Similar to a 2-step phase cycling scheme, the data were collected for 3-step phase cycling at different waiting time and are shown in figure (5.11).

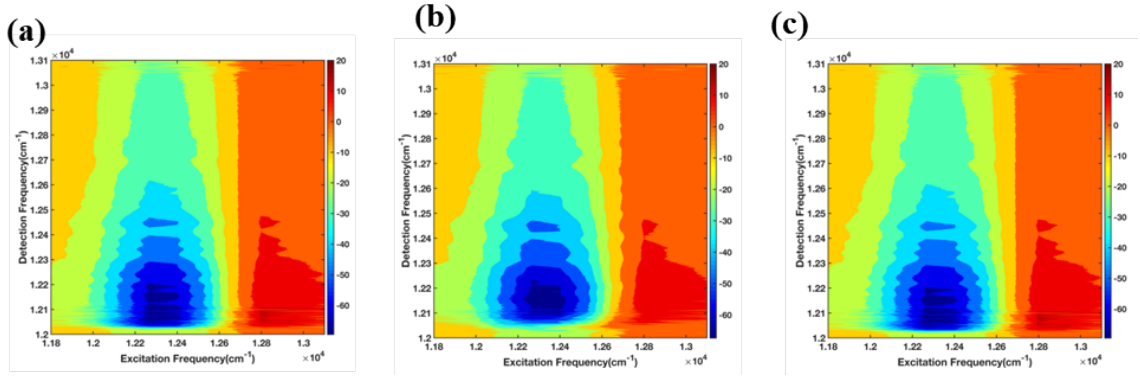

Figure 5.11: 2DES plots for IR-140 at (a) 0 ps (b) 0.1 ps & (c)1 ps using 3 – step phase cycling

For IR140, the laser spectrum overlaps with the blue edge of the emission spectrum, therefore only vibrational relaxation is expected. It is evident from the 2D spectrum of IR140 (for both 2-step and 3-step phase cycling) that only a little spectrum shift is observed

and further shift cannot be probed by the laser. Therefore, IR140 is not an ideal probe to study solvation dynamics for the employed laser wavelength.

5.2.2. DNTTCI

For DNTTCI, the laser spectrum overlaps with the red-edge of absorption and completely overlaps with the emission maximum. Therefore, solvation relaxation can be seen in DNTTCI and hence can be used as an ideal probe for studying solvation dynamics for the employed laser wavelength. The overlap of the laser spectrum with absorption and emission of the dye is shown in figure (4.3).

5.2.2.1. 2DES analysis

Similar to IR140, data was collected for DNTTCI using 2-step phase cycling and are shown in figure (5.12).

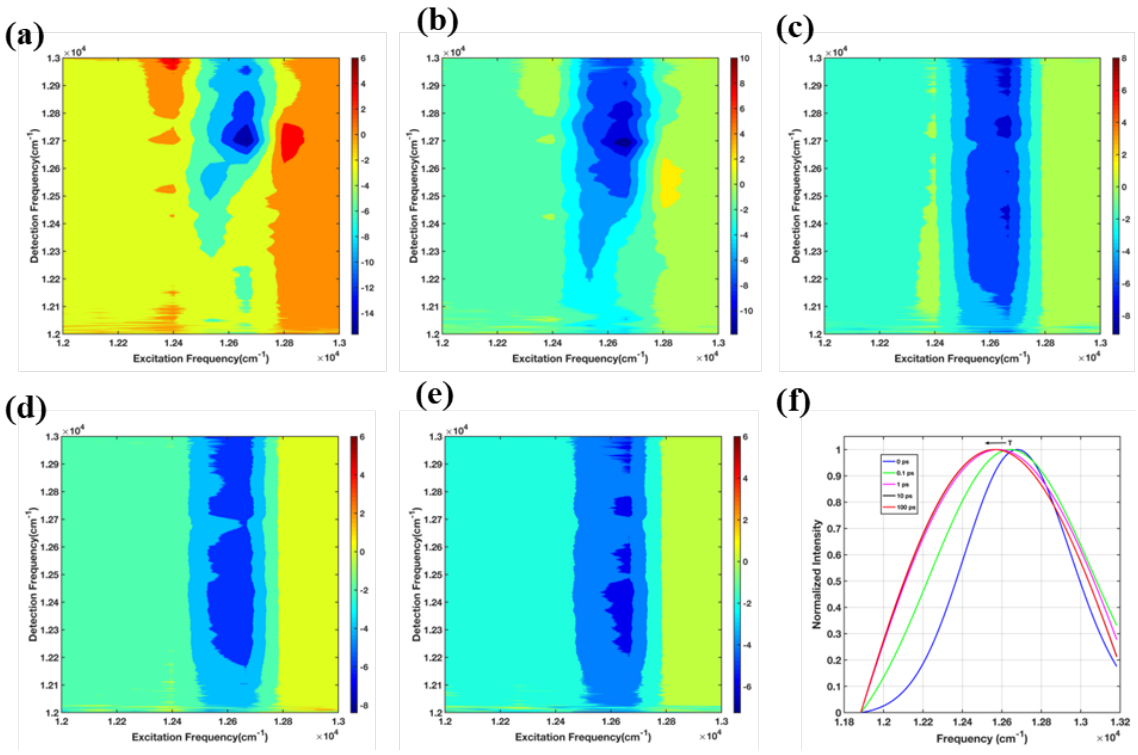

Figure 5.12: 2DES plots for DNTTCI at (a) 0 ps (b) 0.1 ps (c) 1 ps (d) 10 ps (e) 100 ps & (f) the corresponding lognormal fits for selective excitation at 12,530 cm^{-1} using 2 – step phase cycling.

2DES plots for DNTTCI using a three step phase cycling scheme are shown in figure (5.13).

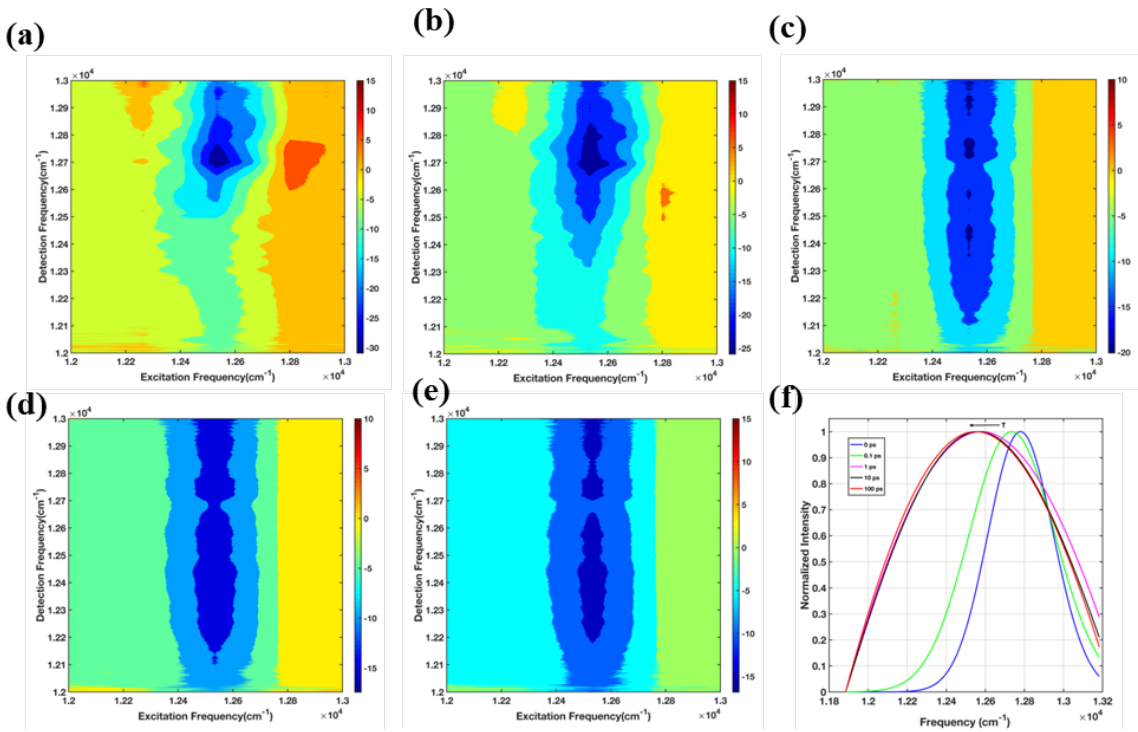

Figure 5.13: 2DES plots for DNTTCI at (a) 0 ps (b) 0.1 ps (c) 1 ps (d) 10 ps (e) 100 ps & (f) the corresponding lognormal fits for selective excitation at 12,530 cm^{-1} using 3 – step phase cycling.

Conclusion

From the 2D Spectra (using both 2-step and 3-step phase cycling) for DNTTCI, spectral shift along the detection axis is seen with waiting/population time. This shift is also clearly visible from the lognormal fits at different waiting times for selective excitation at 12530 cm^{-1}.

Further, excitation wavelength dependent solvation correlation functions can be constructed using 2DES.

Excited State Photophysics

6. **Excited State Dynamics of Polyacenes**

7. **Two Photon Pump and One Photon Probe Studies in Rhodamine 6G**

Excited State Dynamics of Polyacenes

6.1. Introduction

6.1.1. Polyacenes

Polyacenes are a class of organic molecules that are made up of fused benzene rings. The general structure of polyacenes is shown in figure (6.1).

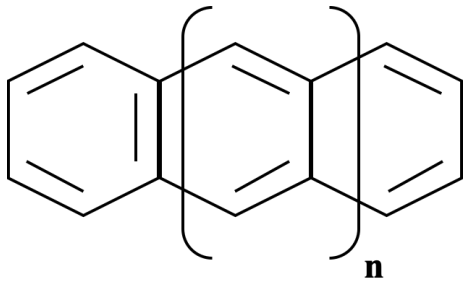

Figure 6.1: General structure of polyacene molecules

Large polyacenes such as tetracene and pentacene are considered as prototypes for conjugated organic semiconductors because of high charge carrier mobility [11]. These molecules are also known to show the process of exciton fission (or singlet fission) in which an excited singlet is split into a pair of triplets. Such process is considered as a promising way to increase the overall efficiency of solar cells. Singlet fission plays an important role in the photophysics and optoelectronic properties of tetracene and pentacene molecules.
In case of pentacene, $\mathbf{E(S1)} > \mathbf{2E(T1)}$ so the formed triplets cannot recombine to form a singlet. In case of tetracene, $\mathbf{E(S1)} \cong \mathbf{2E(T1)}$ so the formed triplets can again combine to form a singlet [12].

6.1.2. Singlet Fission

Singlet fission is process in which a chromophore molecule in its singlet excited state shares its excitation energy with a neighboring chromophore molecule in its ground state such that both the chromophores are converted to triplet excited states [13]. The two chromophore molecules may be of same kind or different kind. In the former case the singlet fission is called as “homofission” while in the latter case, it is called “heterofission”. Singlet fission

is spin allowed process because the two triplets excitations couple together to form a singlet state. The mechanism for singlet fission is shown in figure (6.2). In figure (6.2) chromophore 1 undergoes excitation to the singlet state S_1. It then shares its excitation energy with chromophore 2 such that both chromophores are converted to triplet excited states. The two triplets on each chromophore are coupled together to form a singlet state.

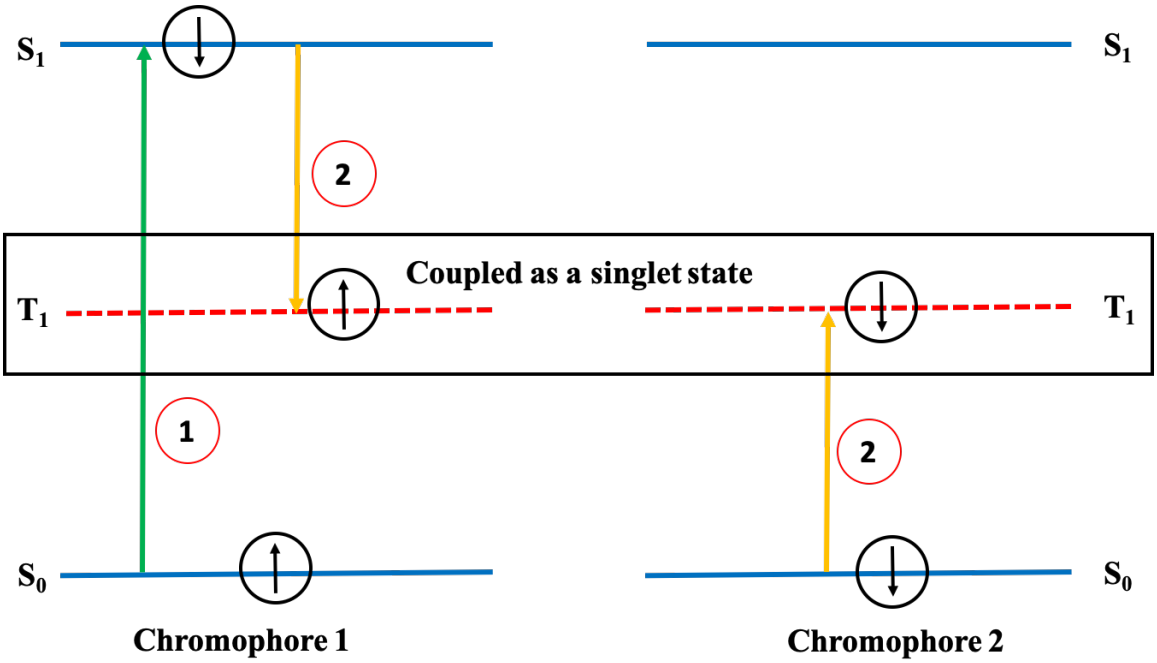

Figure 6.2: Mechanism for singlet fission

The kinetics for singlet fission can be represented as:

$$S_0 + S_1 \underset{\gamma_s}{\overset{\gamma'}{\rightleftharpoons}} T_1 + T_1$$

Where, γ' = rate of singlet fission; γ_s = rate of triplet-triplet annihilation

Singlet fission can also be represented as:

$$S_0 + S_1 \underset{k_{-1}}{\overset{k_1}{\rightleftharpoons}} {}^1(T\,T) \underset{k_{-2}}{\overset{k_2}{\rightleftharpoons}} T_1 + T_1$$

^{1}(TT) = correlated triplet pair = triplet states on two adjacent chromophores coupled together to form a singlet state

$\varepsilon = \frac{k_{-1}}{k_2}$ = branching ratio = probability that ^{1}(TT) comes back to S_1 instead of going to $T_1 + T_1$.

6.1.2.1. Conditions for singlet fission

- Singlet fission does not take place in single small molecules and usually occurs in multichromophoric systems as it requires at least two excitation sites to accommodate the triplet excitations formed. For very large polyenes, the two choromophoric units can be in the same molecule.
- Singlet fission can be observed in solutions of chromophores if the fluorescence lifetime of the chromophores is long and the ground state concentration is high enough to have diffusive encounters between the S_0 and S_1 states of the chromophores.
- If the energy of lowest lying singlet state ($E(S_1)$) is less than twice the triplet excitation energy ($2E(T_1)$) then the singlet fission cannot take place without any thermal activation. It can occur from a higher lying singlet state (S_n) or a vibrationally excited S_1 but the process of singlet fission then has to compete with internal conversion and vibration relaxation.
- For efficient singlet fission to take place the following condition should be met

$$\mathbf{E(S_1) \geq 2E(T_1)}$$

- For the observation of singlet fission, the initially formed triplets should diffuse apart very quickly (e.g. in case of solids and conjugated polymers) If the formed triplets do not diffuse apart, they can be destroyed by the process of triplet-triplet annihilation which can then form an excited singlet or a higher lying singlet.

6.2. Results and discussion

Excited state dynamics of both tetracene and pentacene were studied using femtosecond visible transient absorption spectroscopy.

6.2.1. Tetracene

Tetracene belongs to the class of polyacenes. It is a Centro-symmetric molecule belonging to the D_{2h} symmetry point group.

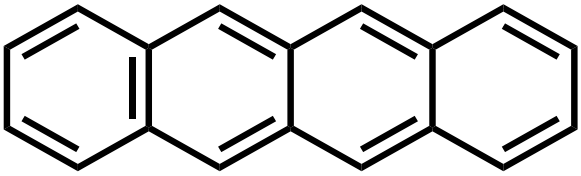

Figure 6.3: Molecular structure of tetracene

Tetracene (Benz[b]anthracene) sublime grade was purchased from Sigma Aldrich and was used as such. It was dissolved in toluene to make a solution of $5 \times 10^{-4}\, M$ concentration.

6.2.1.1. Steady state analysis

Steady state absorption measurements were taken using Lab India UV-Vis spectrometer using a 2 mm path length cuvette and the steady state fluorescence spectra were taken using Shimadzu Spectrofluorometer.

The steady state absorption spectra are shown in the figure (6.4).

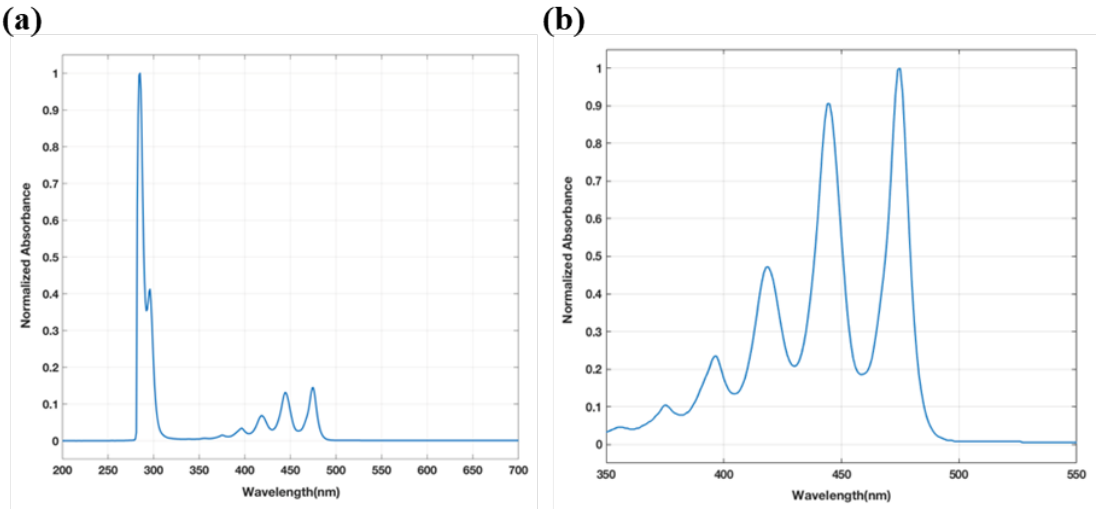

Figure 6.4: (a) UV-Vis Absorption Spectra of tetracene (b) visible Absorption Spectra of tetracene in visible region

The absorption spectra of tetracene show the maximum absorbance at 285 nm which corresponds to the absorption from ground state to some higher lying singlet($S_0 \rightarrow S_n(n > 1)$). Absorption spectrum in the visible region clearly shows vibronic progressions with maxima at 475 nm (corresponding to the 0-0 transition). The other absorption peaks are at 445 nm, 418 nm, 397 nm and 375 nm.

The fluorescence emission spectra of tetracene were taken by exciting the sample at different absorption maxima of the sample.

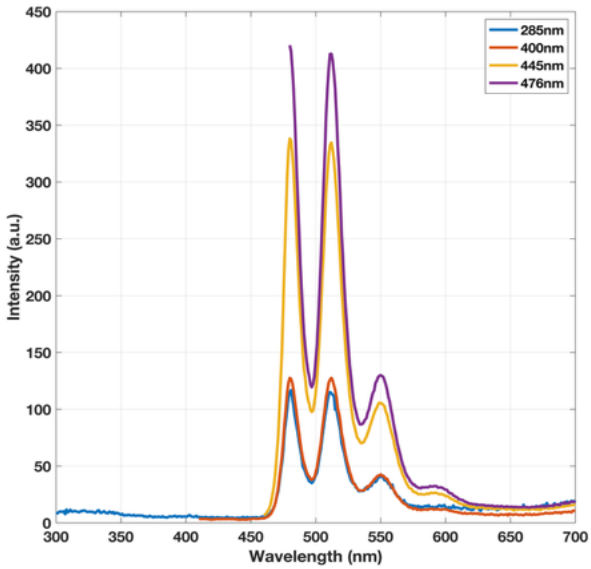

Figure 6.5: Emission Spectrum of tetracene at different excitation wavelengths

From the emission spectra, it is seen that maximum fluorescence emission at 480 nm takes place at excitation wavelength of 475 nm. Other emission peaks are at 512 nm and 551 nm. Also, the vibronic features present in the absorption spectrum are reflected in the emission spectrum.

The excitation spectrum at different emission maxima of the sample was taken and is shown in figure (6.6).

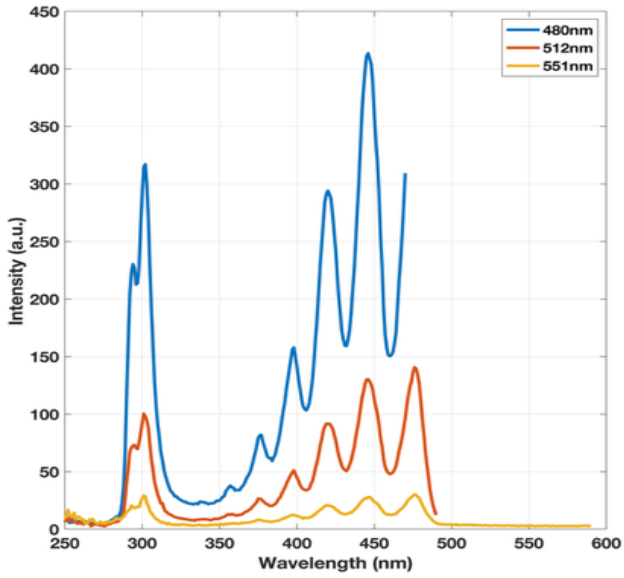

Figure 6.6: Excitation Spectrum of tetracene at different emission wavelengths

Fluorescence emission spectra with varying concentration were taken and are shown in figure (6.7).

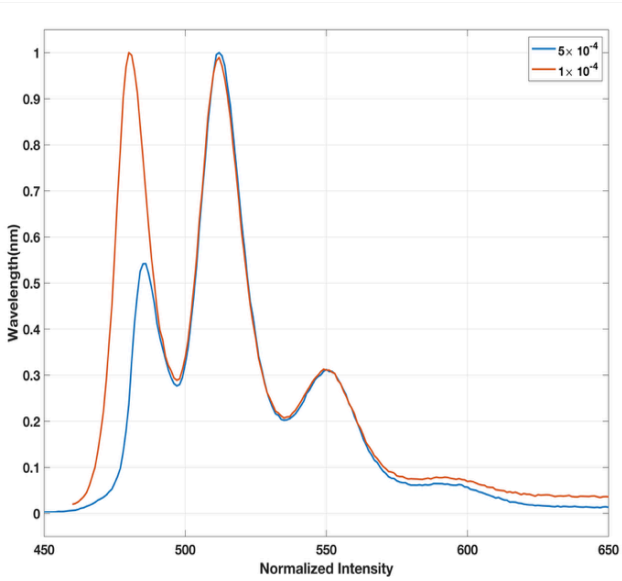

Figure 6.7: Fluorescence spectra with varying concentration

From figure (6.7), it can be seen that with increase in concentration the intensity of emission at 480 nm is decreased. This may be attributed to inner filter effect.

The steady state measurements (both absorbance and fluorescence) are summarized in figure (6.8).

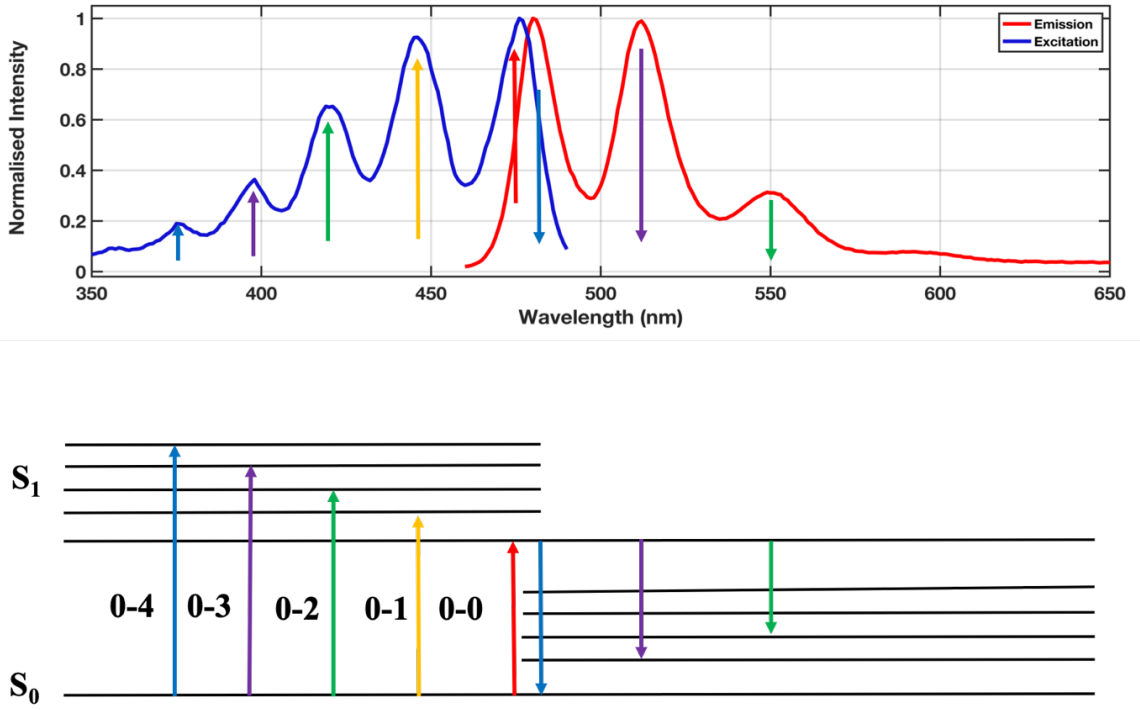

Figure 6.8: Summary of steady state measurements

From figure (6.8), it can be seen that the absorption and emission spectra are mirror image of each other. This implies that nuclear geometry of the molecule does not change much during the electronic excitation.

6.2.1.2. Pump – probe analysis

A 1 kHz repetition rate amplified Ti: Sapphire system (Libra, Coherent) was used as the laser source with a central wavelength at ~ 800 nm and pulse width ~55 fs.

Beam splitters were used to split the 800 nm beam into the pump and the probe. The pump and probe were routed to femtosecond transient absorption spectrometer (TAS, Newport Corp.) A type-I BBO was inserted into the pump arm to generate 400 nm pump pulse (second harmonic generation) and a calcium fluoride (CaF_2) plate was employed to generate white light continuum which was then used as the probe pulse. The pump and the probe were overlapped inside the sample. The delay between the pump and the probe was controlled using a mechanical delay stage (ILS300LM, Newport Corp.) which can provide a delay of up to 4ns with a minimum step size of ~0.13 fs. A mechanical chopper (New Focus 3502) running at a repetition of 500 Hz was used which blocks every alternate pump

pulse to generate differential absorption signal (ΔOD/ΔA) at each pump – probe delay. The transmitted probe was sent then sent to a spectrometer.

The overlap of the pump and the probe with the absorption and emission spectrum of tetracene are shown in figure (6.9).

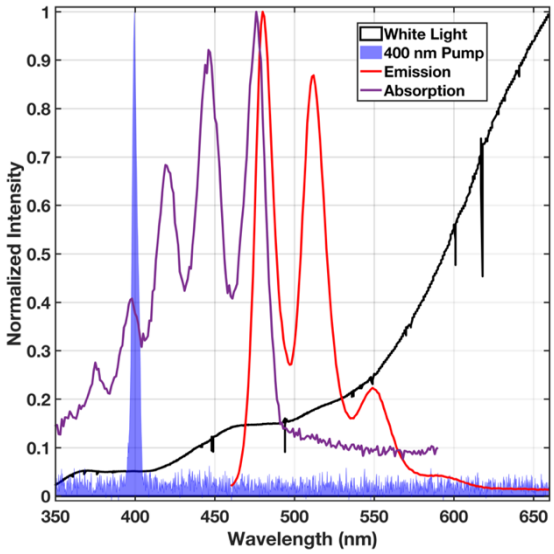

Figure 6.9: Overlap of absorption and emission spectrum with laser (pump and probe) spectrum

The 400 nm pump overlaps with the absorption peak at 397 nm while the white light probe overlaps with complete absorption and emission spectrum.

The pump – probe signal as a function of both pump – probe delay and probe wavelength is shown in figure (6.10).

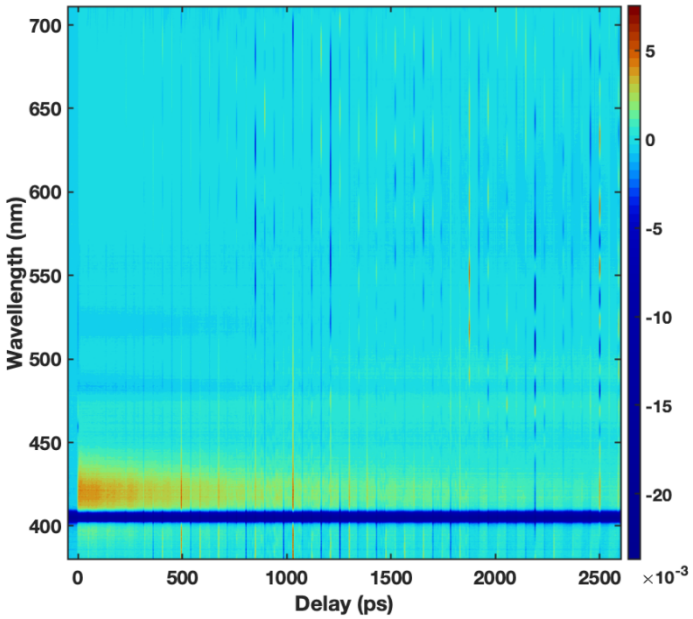

Figure 6.10: Pump probe signal as a function of both pump – probe delay and probe wavelength

In the pump probe signal (figure (6.10)), a continuous patch at ~ 400 nm is due to pump scattering. The signal is dominated by an ESA in the range ~410 – 450 nm.

The low signal to noise ratio in the pump –probe may be due to:

- Domination of the signal by ESA feature in the range ~410 – 450 nm.
- Not exciting the sample at its absorption maxima.
- Low extinction coefficient (i.e. 2500 $^{-1}$ cm^{-1}) at 397 nm.

The spectral traces at different delays between pump and the probe are shown in figure (6.11).

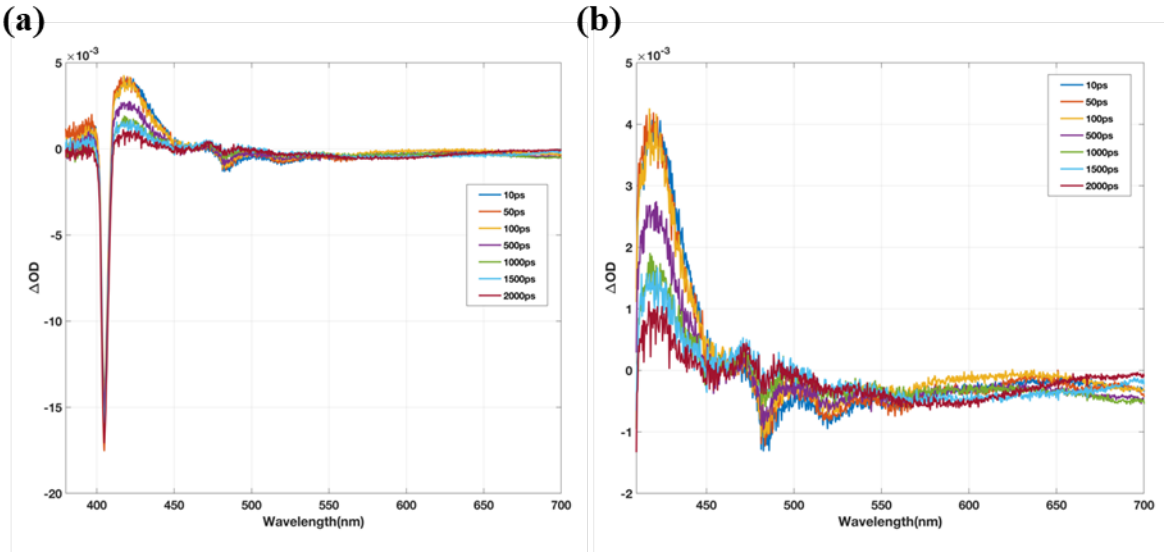

Figure 6.11: Spectral traces at various pump – probe delays (a) with pump scatter (b) without pump scatter

From the spectral traces shown in figure (6.11), it is clear that the signal is dominated by an ESA at ~ 420 nm.

Other features in the transient absorption spectrum are the SE at ~ 483 nm, ESA at ~ 452 nm and ~617 nm.

Spectral traces shown in figure (6.11) are at the pump probe delays of 10 ps, 50 ps, 100 ps, 500 ps, 1000 ps, 1500 ps and 2000 ps. At the features in transient absorption spectrum are decaying with increase in pump probe decay except for the ESA feature at ~ 452 nm which shows some initial rise in the signal.

Further, the kinetic traces for different signals are shown in figure (6.12) – figure (6.14). Figure (1.12) is the kinetic trace for ESA at 423 nm, figure (6.13(a)) is kinetic trace for SE at 483 nm, figure (6.13(b)) is the kinetic trace for ESA at 617 nm and figure (6.14) is the kinetic trace for ESA at 452 nm.

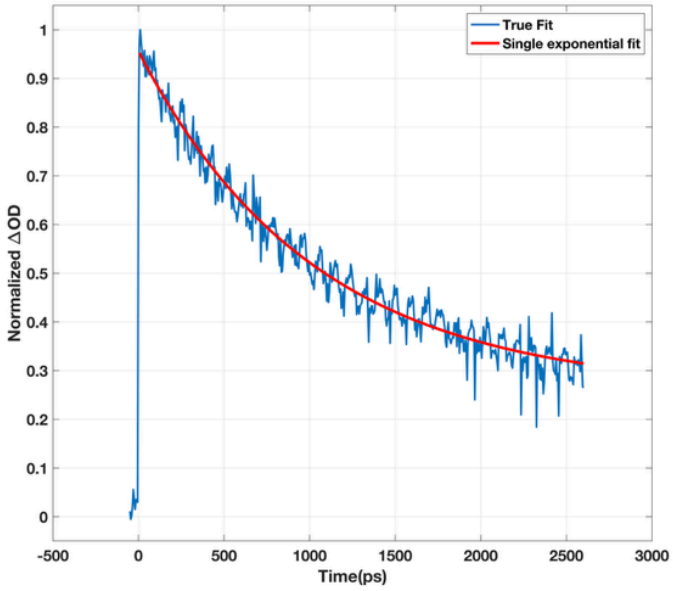

Figure 6.12: Kinetic traces for excited state absorption at 423 nm

The kinetic decay was fitted to an equation of mono-exponential decay of type:

$$y = y_0 + A \times \exp\left(\frac{-x}{t_1}\right)$$

ESA at 423 nm			
A	y_0	t_1 (ps)	R^2
0.4	0.4	1023	0.80

Table 6.1: Parameters for Kinetic trace of excited state absorption at 423 nm

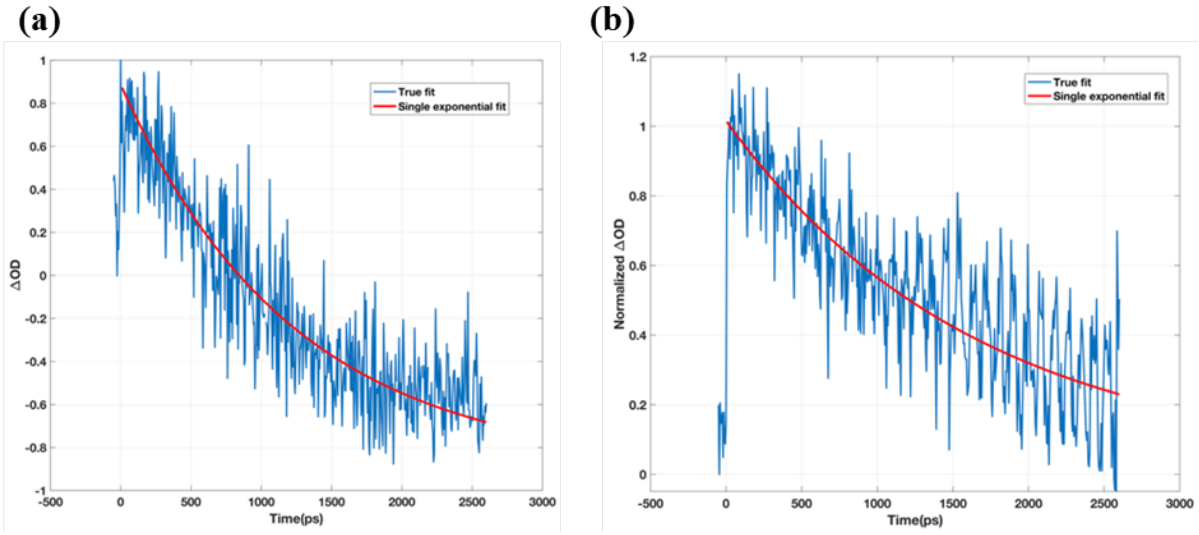

Figure 6.13: Kinetic traces for (a) Stimulated emission at 483 nm (b) Excited state absorption at 617 nm

The kinetic decays were fitted to an equation of mono-exponential decay of type:

$$y = y_0 + A \times \exp\left(\frac{-x}{t_1}\right)$$

SE at 483 nm				ESA at 617 nm			
A	y_0	t_1 (ps)	R^2	A	y_0	t_1 (ps)	R^2
0.135	0.278	816	0.25	0.08	0.73	1144	0.30

Table 6.2: Parameters for Kinetic traces of Stimulated emission at 483 nm and excited state absorption at 617 nm

The reported value for Fluorescence lifetime of tetracene in solution is ~4.2 ns [14] but the stimulated emission signal at ~483 nm decays with a time constant of ~ 816 ps which is much faster than the fluorescence lifetime of tetracene in solution. This rapidly decaying stimulated emission signal suggests the presence of some other process that may be competing with fluorescence.

Apart from rapidly decaying SE signal, there is an ESA signal at ~452 nm with a very long time constant of ~423 ns which is shown in figure (6.14).

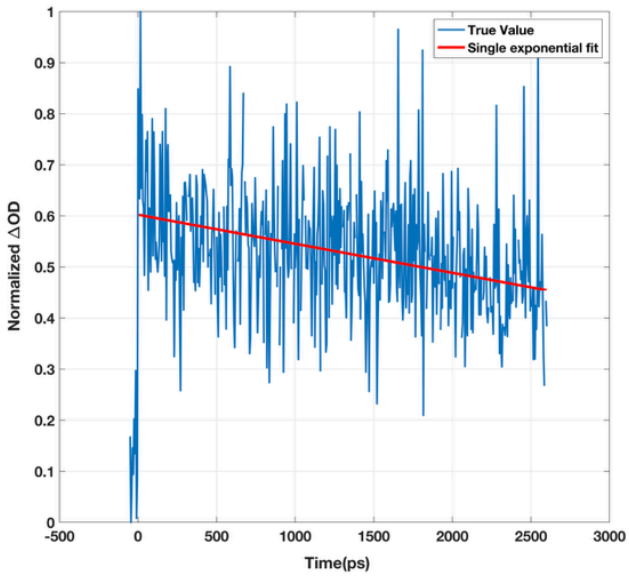

Figure 6.14: Kinetic traces for excited state absorption at 452 nm

ESA at 452 nm			
A	y_0	t_1 (ps)	R^2
2.4	-6.3	423	0.17

Table 6.3: Parameters for Kinetic trace of excited state absorption at 452 nm

In case of solution, the initially formed triplets can be destroyed due to triplet – triplet annihilation and then form an excited singlet state. The longer time constant at 452 nm can be due ESA from the singlet excitation formed due to annihilation of initially formed triplets (a process similar to reverse intersystem crossing). The schematic for triplet – triplet annihilation is shown in figure (6.15).

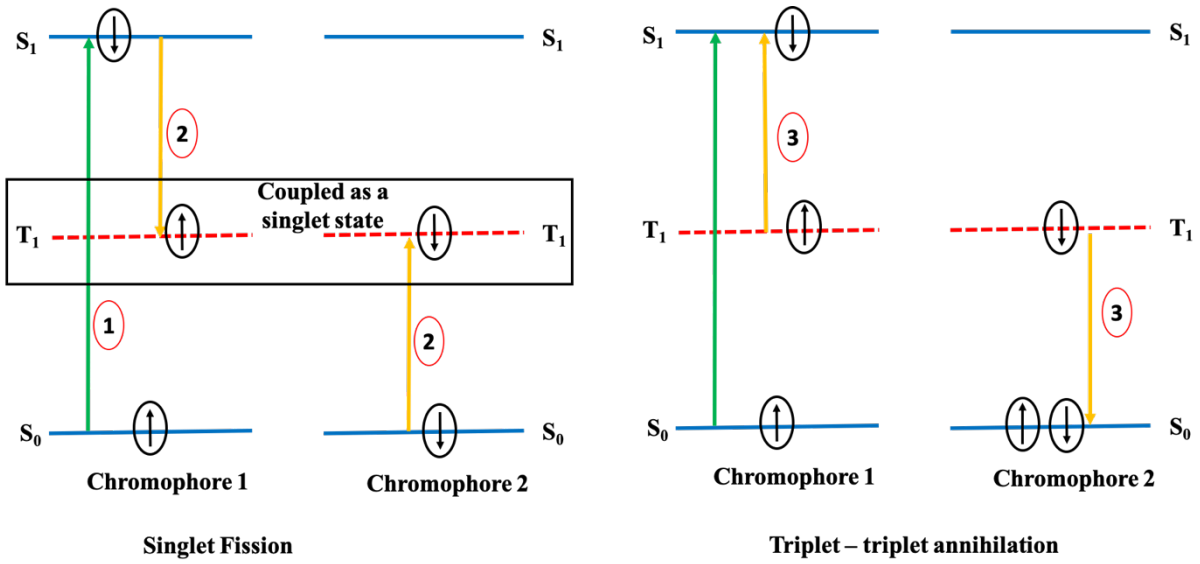

Figure 6.15: Triplet – triplet annihilation after formation of correlated triplet pair

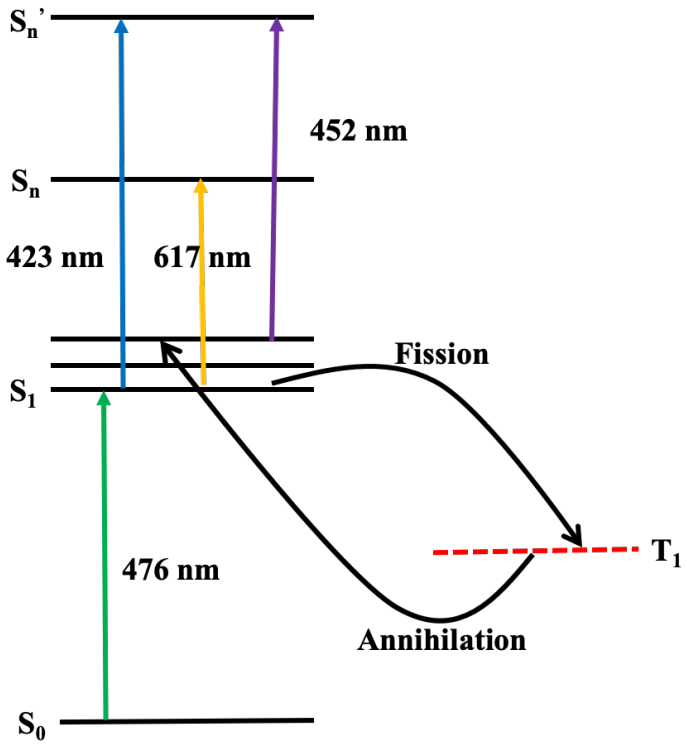

Figure 6.16: Electronic States of tetracene

6.2.2. Pentacene

Similar to tetracene, pentacene also belongs to the class of polyacene molecules having D_{2h} point group symmetry.

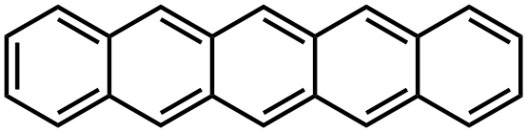

Figure 6.17: Molecular structure of pentacene

Films of pentacene were prepared by drop casting the solution of pentacene in chloroform using a spin coater and the solvent was then allowed to evaporate.

6.2.2.1. Steady state analysis

The steady state absorption spectra of pentacene are shown in the figure (6.18).

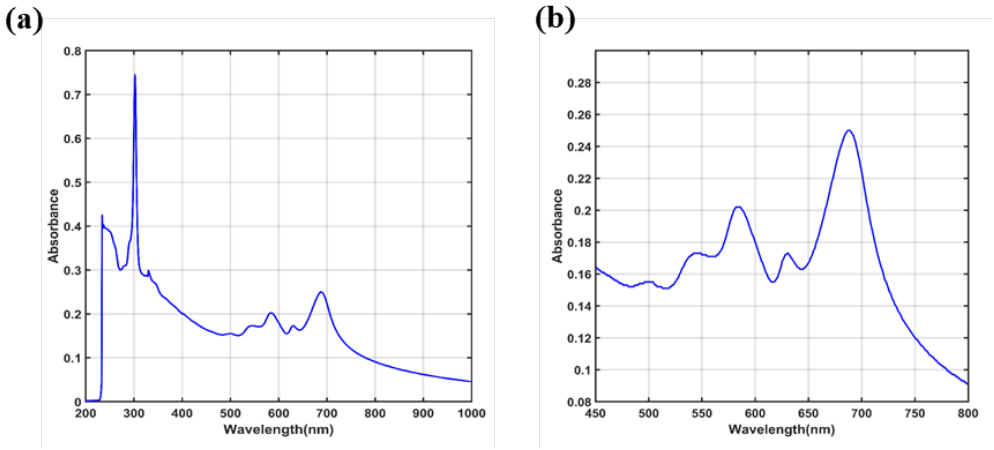

Figure 6.18: (a) UV-Vis absorption spectra (b) visible absorption spectrum of pentacene

The fluorescence emission spectra for pentacene at different excitation wavelengths are shown in figure (6.19).

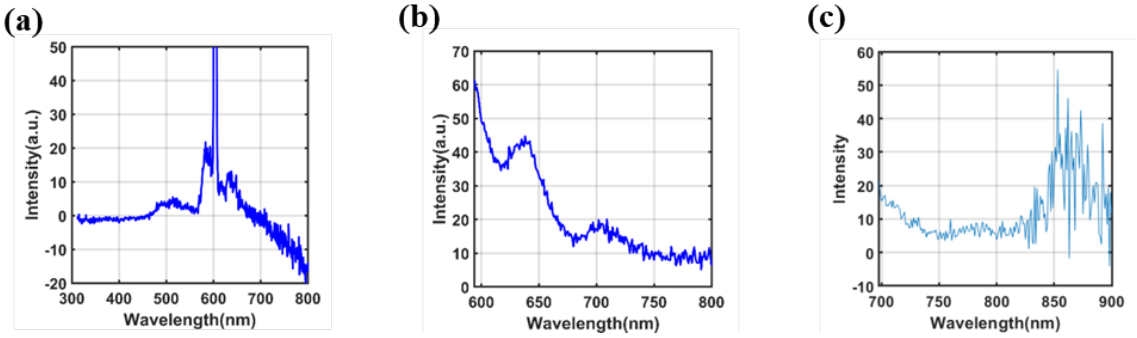

Figure 6.19: Emission spectrum of pentacene for excitation wavelength at (a) 302 nm (b) 584 nm & (c) 688 nm

The fluorescence spectrum of pentacene indicates that it has very low or negligible fluorescence emission.

6.2.2.2. Transient Absorption Studies

The transient absorption studies for pentacene films was done by exciting the sample with a ~600 nm pump pulse generated using NOPA (TOPAS White, Light Conversion) and a white light probe.

The pump – probe signal as a function of both pump – probe delay and probe wavelength is shown in figure (6.20).

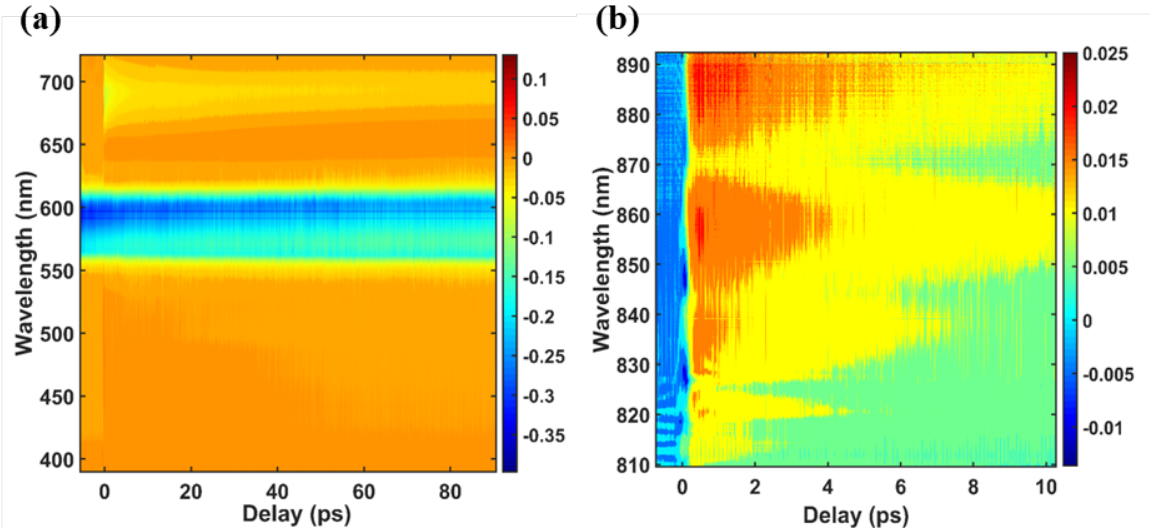

Figure 6.20: Pump probe signal as a function of both pump – probe delay and probe wavelength in the range of (a) 380 – 720 nm & (b) 810 – 900 nm

The spectral traces at different delays between pump and the probe are shown in figure (6.21).

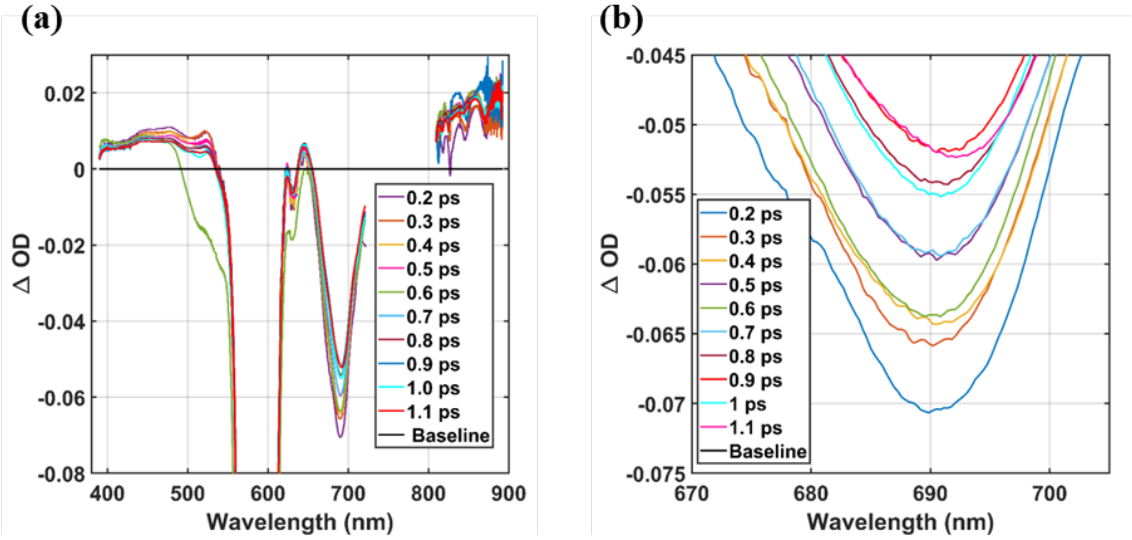

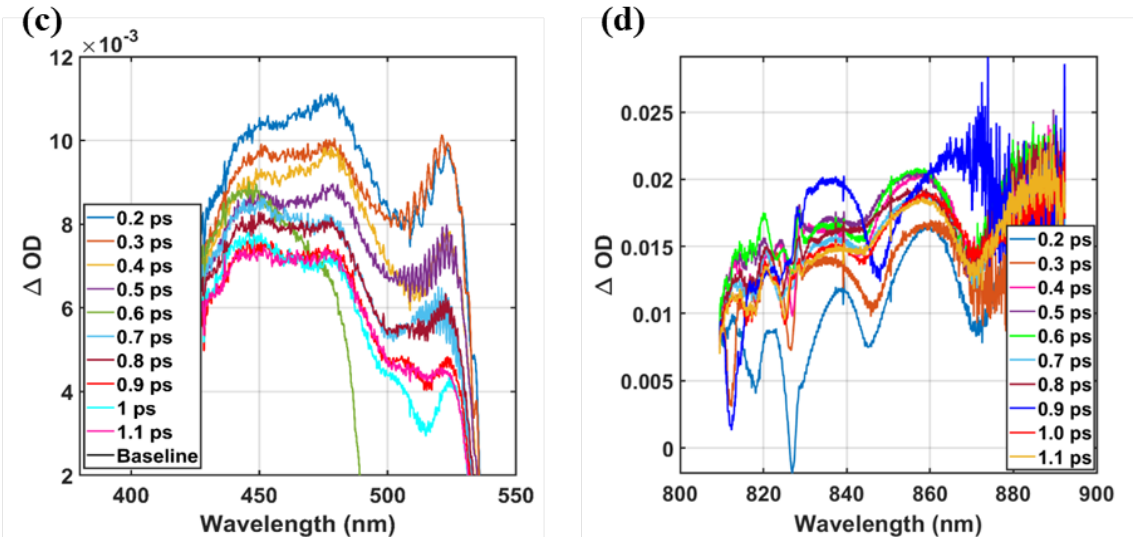

Figure 6.21: Spectral traces for the different pump probe signals (a) complete trace (b) SE + GSB centered at 690 nm (c) ESA centered at 450 nm & (d) ESA centered at 850 nm

From the spectral traces of SE + GSB at 690 nm and ESA at 450 nm, it can be clearly seen that the intensity of spectra decreases with increase in the delay between the pump and the probe but for ESA at 850 nm, the intensity of spectra increases up to 0.9 ps and then decreases which clearly indicates that there is some rise component associated with this signal. The kinetics of each of these spectral features is shown in figure (6.22) and figure (6.23).

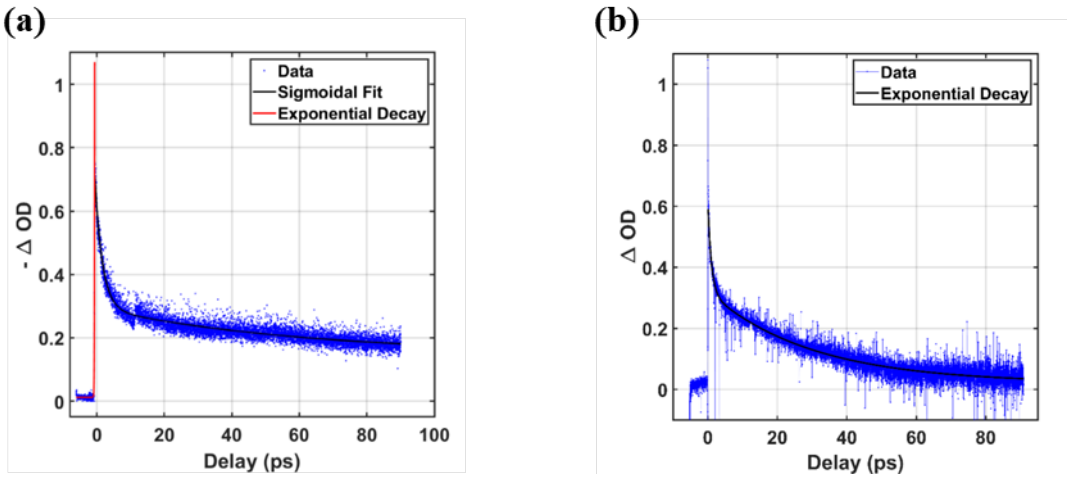

Figure 6.22: Kinetic traces for (a) SE at 690 nm & (b) ESA at 458 nm

Bi-exponential fit for SE at 690 nm				Bi-exponential fit for ESA at 458 nm			
A_1	t_1 (ps)	A_2	t_2 (ps)	A_1	t_1 (ps)	A_2	t_2 (ps)
0.32	2.21	0.14	60.41	0.23	1.01	0.29	29.66

Table 6.4: Parameters for Kinetic trace of SE at 690 nm & ESA at 458 nm

From the kinetic parameters of E at 690 nm, it can be seen that it has a very fast decay rate of 2.2 ps which shows that one of the components of SE is decaying at a very fast rate. The similar dynamics can be seen for ESA at 458 nm which also has a very fast decaying rate of 1 ps.

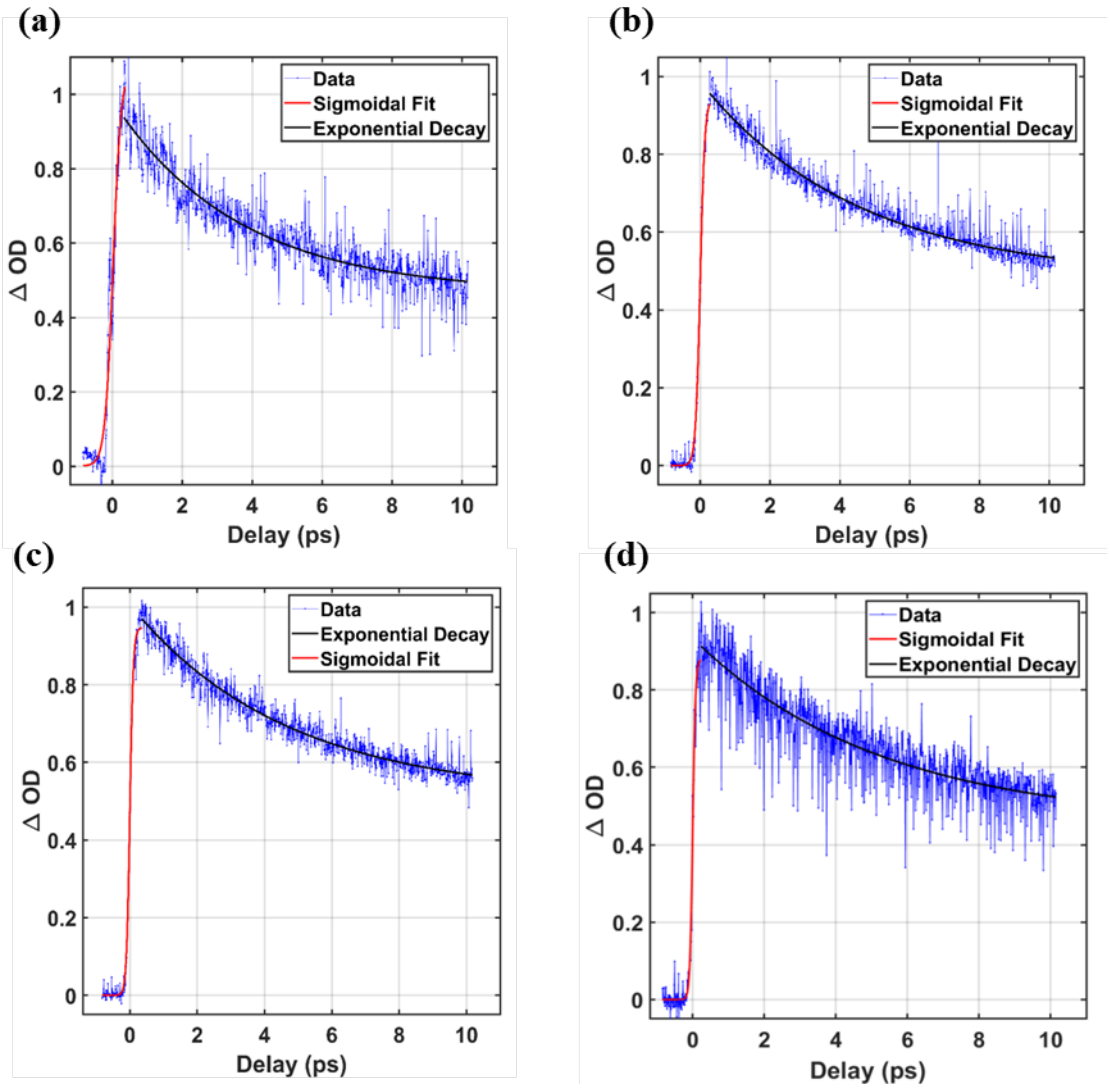

Figure 6.23: Kinetic traces for (a) ESA at 815 nm (b) ESA at 836 nm (c) ESA at 858 nm & (d) ESA at 879 nm

The parameters for the fitting of mono-exponential decays are shown table (6.5).

Exponential decays											
ESA at 815 nm			**ESA at 836 nm**			**ESA at 858 nm**			**ESA at 879 nm**		
A_1	y_0	t_1 (ps)	A_1	y_0	t_1 (ps)	A_1	y_0	t_1 (ps)	A_1	y_0	t_1(ps)
0.49	0.46	3.59	0.53	0.48	4.52	0.49	0.51	4.64	0.49	0.45	5.21

Table 6.5: Parameters for decay of kinetic trace of ESA at 815 nm, 836 nm, 858 nm & 879 nm

From the spectral traces in the region of 810 – 900 nm as well as the kinetic traces for this region, it can be seen that there is rise component associated with the signal observed in the region of 810 – 900 nm. This rise in the kinetic traces is fitted with a sigmoidal equation to obtain the rate at which these signals grow/rise and are shown in figure (6.24).

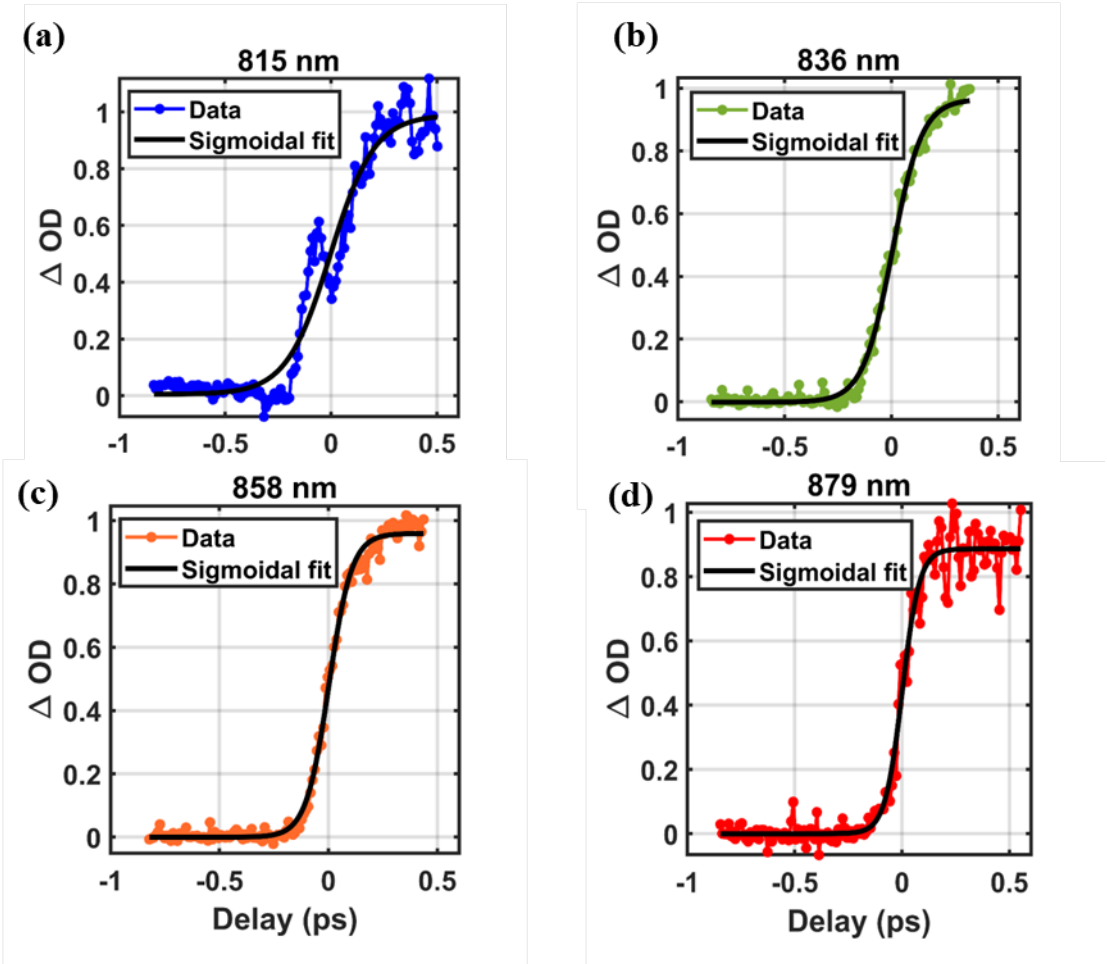

Figure 6.24: Sigmoidal fits for the rise of ESA at (a) 815 nm (b) 836 nm (c) 858 nm & (d) 879 nm

Sigmoidal fits for rise							
ESA at 815 nm		**ESA at 836 nm**		**ESA at 858 nm**		**ESA at 879 nm**	
A_2	dx (ps)	A_2	dx (ps)	A_2	dx (ps)	A_2	dx (ps)
1.1	0.116	0.94	0.066	0.95	0.051	0.88	0.039

Table 6.6: Parameters for sigmoidal fit of ESA at 815 nm, 836 nm, 858 nm & 879 nm

From the parameters of sigmoidal fits in table (6.6), it can be seen that there is a rise component associated with the ESA signals in the range of 810 – 900 nm. The rise time is slower for the blue wavelengths and is faster for red wavelength which is contrary to SE signals where red has a slower rise time and blue has a faster rise time. Since the signal in the range 810 – 900 nm is attributed to a triplet state [15], the growth time for these states corresponds to the triplet buildup from the singlet. Also, the slower rise for blue wavelength suggests that the population from the singlet state is transferred to some higher vibrational level of the triplet state.

Conclusion

The absence of very low steady state emission, very fast decay of singlet SE (at 690 nm) and very fast rise component (40 – 110 fs) for ESA from a triplet state suggests very fast and robust singlet fission in case of pentacene

Two - Photon Pump and One - Photon Studies in Rhodamine 6G

7.1. Introduction

Two-photon absorption is a third order ($\chi^{(3)}$) nonlinear process where an atom/ molecule makes a transition from ground state to an excited state by simultaneously absorbing two laser photons [16]. The molecule makes the transition from ground state to an excited state through an intermediate state (also called as a virtual state).

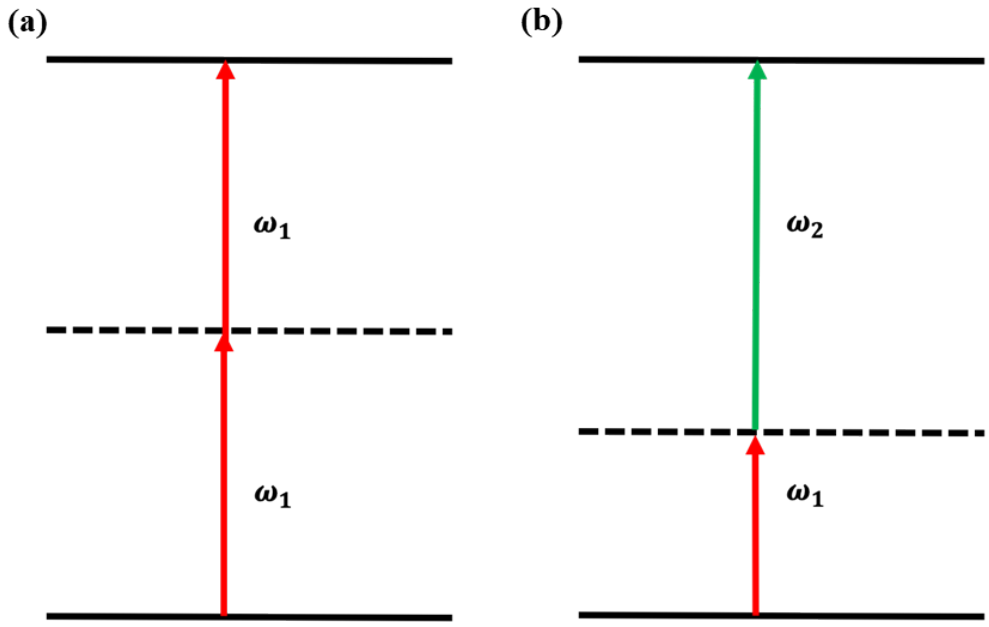

Figure 7.1: Energy level diagram for (a) degenerate two-photon absorption & (b) two-color (non-degenerate) two-photon absorption

The concept of two-photon absorption was first proposed by Maria Goeppert Mayer in 1931 in her doctoral dissertation. The probability for 2PA was also derived by Maria Goeppert Mayer but it was too small to be measured by any incoherent source of excitation. Because of this, no experimental 2PA could be observed until invention of laser in 1960 [16].

It was in 1961; one year after the invention of first laser by Theodore Maiman that the first observation of 2PA-induced fluorescence in Eu^{+2} doped CaF_2 crystal was reported by Kaiser and Garrett [17].

7.1.1. Theoretical formulation of TPA parameters

The change in intensity of absorbed light (I) with the position (z) is given as:

$$\frac{\mathbf{dI(z)}}{\mathbf{dz}} = -\boldsymbol{\alpha}\mathbf{I(z)} - \boldsymbol{\beta}\mathbf{I^2(z)} - \boldsymbol{\gamma}\mathbf{I^3(z)} - \boldsymbol{\eta}\mathbf{I^4(z)} \quad \textbf{(7.1)}$$

I(z) = intensity of incident light propagating along z-axis
α, β, γ, and η = One, two, three and four photon absorption coefficients respectively

If only TPA term survives:

$$\frac{dI(z)}{dz} = -\boldsymbol{\beta} I^2(z) \quad \textbf{(7.2)}$$

Equation (7.2) shows that the TPA probability of an atom/molecule is proportional to the square of the intensity of light.

The solution of equation (7.2) is:

$$I(z, \lambda) = \frac{I_0(\lambda)}{1+\beta(\lambda) I_0(\lambda) z} \quad \textbf{(7.3)}$$

Where, $I_0(\boldsymbol{\lambda})$ is the intensity of incident light
β is the TPA coefficient of a material which is macroscopic parameter. It is connected to the concentration of two-photon absorbing molecules as:

$$\beta(\lambda) = \frac{\sigma_2(\lambda) N_A d_0}{h\nu \times 10^3} \quad \textbf{(7.4)}$$

N_A = Avogadro number; d_0 = concentration of absorbing molecules (in M)
σ_2 = TPA cross section

Unit of TPA cross-section

$$\mathbf{Rate} \propto \mathbf{I^2}$$
$$= \boldsymbol{\sigma_2} \times \mathbf{I^2}$$

Rate = photon s^{-1}, I = photon s^{-1} cm^{-2}

$$\boldsymbol{\sigma_2} = \frac{\mathbf{Rate}}{\mathbf{I^2}} = \frac{\mathbf{photon\ s^{-1}}}{\mathbf{photon^2 \times s^{-2} \times cm^{-4}}} = \mathbf{cm^4 s (photon)^{-1}} \quad \textbf{(7.5)}$$

Since, TPA cross section of molecules are very low, therefore, another unit for TPA cross section called as GM (after the name of its discoverer, Maria Goeppert Mayer) is commonly used.

$$\mathbf{1\ GM = 10^{-50} cm^4 s (photon)^{-1}} \quad \textbf{(7.6)}$$

7.1.2. One photon excitation vs. Two photon excitation

- For molecules with no center of symmetry having one photon allowed transitions can show non negligible two-photon transitions if there is a change in dipole moment during excitation [18].
- For molecules like coumarin 307, the state reached by OPE and TPE are identical.
- For molecules like Fluorescein and Rhodamine B, the TPE wavelengths are blue shifted with respect to OPE.

Dye molecule	2 × OPE wavelength (nm)	TPE wavelength (nm)
Coumarin 307	790	776
Rhodamine B	1024	782
Fluorescein	1104	840

Table 7.1: OPE vs. TPE wavelengths

- For molecules in which TPE spectra are blue shifted, some higher excited singlet state can be reached with greater probability by TPE than by OPE.
- OPE induced fluorescence occurs throughout the sample thickness while TPE induced fluorescence is localized to focal volume.

Area dependency of rate of OPE and TPE induced fluorescence can be shown as follows:

For One photon absorption:

$$\boldsymbol{Rate} \propto \boldsymbol{I \times N = \frac{P}{A} \times (\rho \times A) = P \times \rho} \quad \textbf{(7.7)}$$

Two photon absorption:

$$\boldsymbol{Rate} \propto \boldsymbol{I^2 \times N = \frac{P^2}{A^2} \times (\rho \times A) = \frac{P^2}{A} \times (\rho)} \quad \textbf{(7.8)}$$

Where, ρ = number density = N/A, P = optical power

From equation (7.7) and (7.8), it can be seen that rate of OPA has no area dependence while rate of TPA is inversely proportional to the area; therefore, TPA is higher at focal volume due to smaller area.

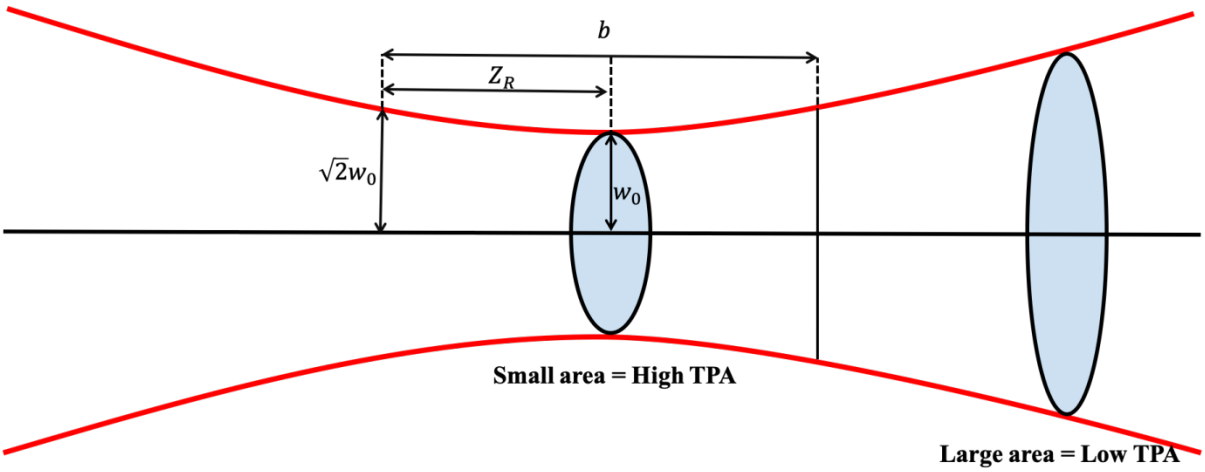

Figure 7.2: Variation of TPA with area

Where, Z_R = Rayleigh length = distance along the direction of propagation of beam from the waist to the place where the area of cross section is doubled = $\frac{\pi w_0^2}{\lambda}$

λ = wavelength; w_0 = beam waist

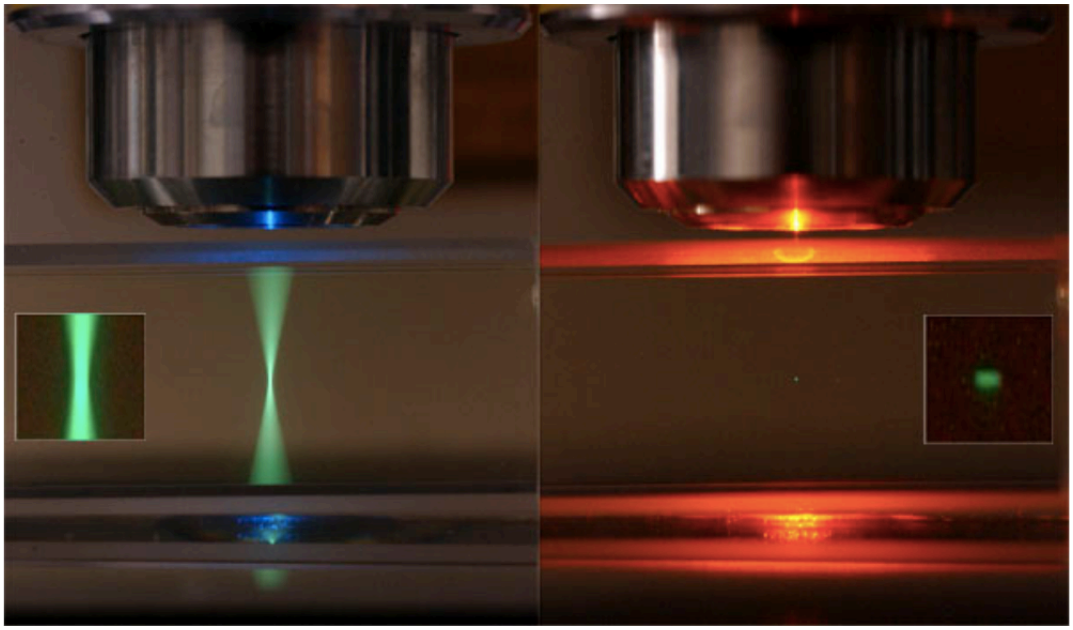

Figure 7.3: One photon vs. two photon fluorescence [19]

- For molecules with center of inversion, states which are not accessible with OPA (due to parity restrictions) can be accessed with TPA.
- In addition to parity restrictions, factors such as vibronic coupling can alter the inversion symmetry and partially allow the parity forbidden transitions.

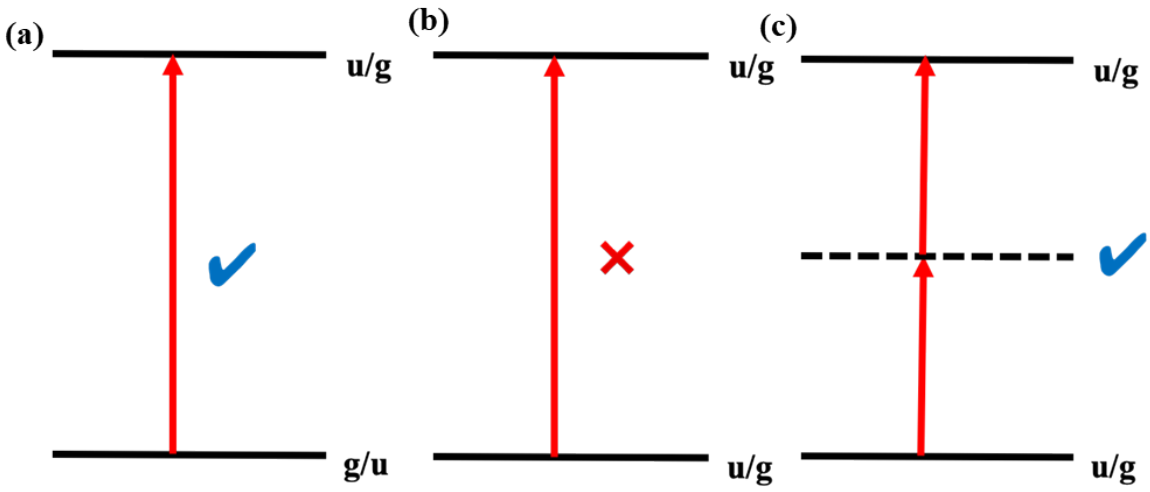

Figure 7.4: Parity rules for molecules with center of inversion

7.2. Results and Discussion

7.2.1. Steady state analysis

From equation (7.4), it can be seen that that TPA coefficient β is directly proportional to the concentration of absorbing molecules. To have significant TPA, a concentrated (10^{-4}M) solution of Rhodamine 6G was used. To check if there is any aggregation on increasing concentration, the absorption spectrum at different concentrations was taken.

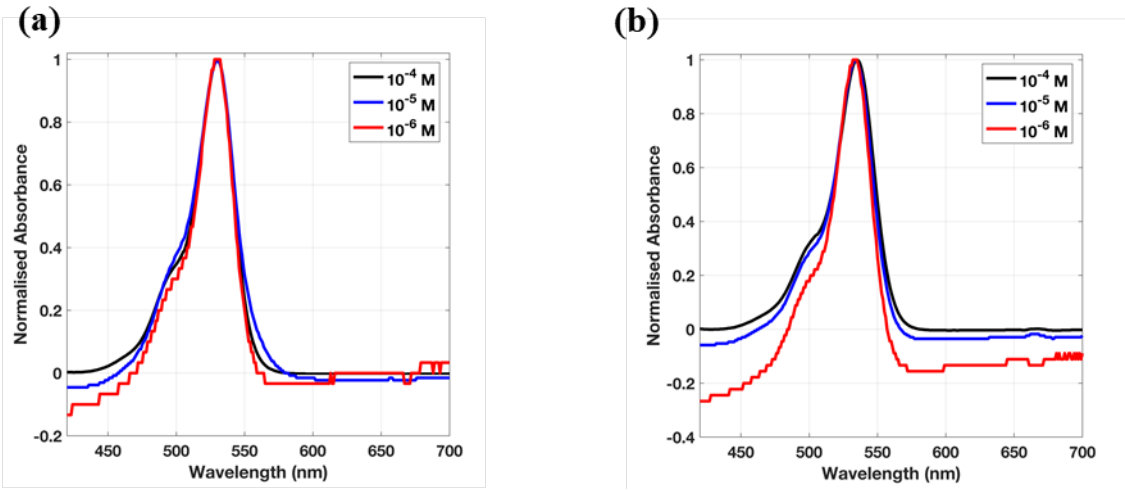

Figure 7.5: Absorption spectrum of Rhodamine 6G with varying concentration in (a) ethanol & (b) Ethylene Glycol

From the figure (7.5), it can be seen there are no significant differences in the absorption spectrum with increasing concentration.

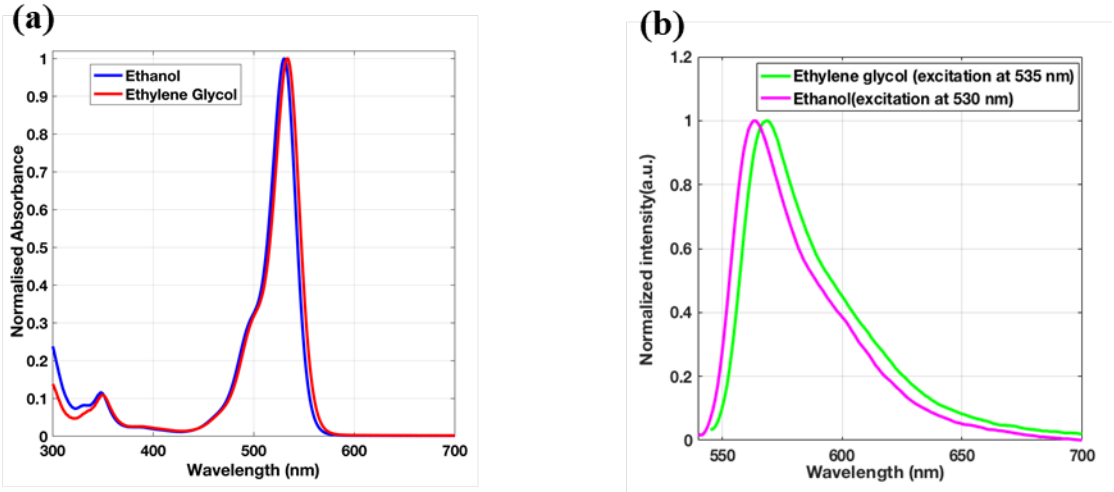

Figure 7.6: (a) Absorption spectrum of Rhodamine 6G (b) emission spectrum of Rhodamine 6G

Absorption maxima in ethanol = 530nm

Emission maxima in ethanol = 564nm (excitation at 530nm)

Absorption maxima in ethylene glycol = 535nm

Emission maxima in ethylene glycol = 567nm (excitation at 535nm)

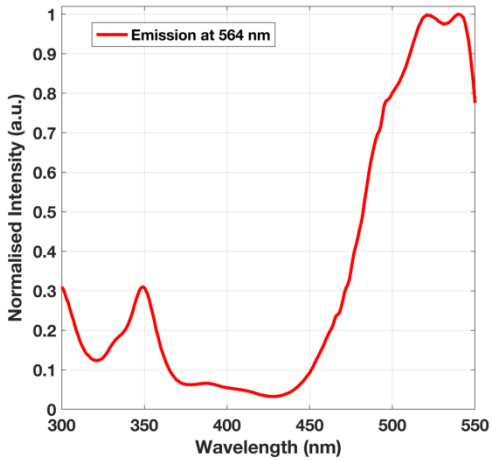

Figure 7.7: Excitation spectrum of Rhodamine 6G in ethanol with emission at 564 nm

To explore the one photon allowed states, the Fluorescence emission spectra at different excitation wavelengths were taken and are shown in figure (7.8).

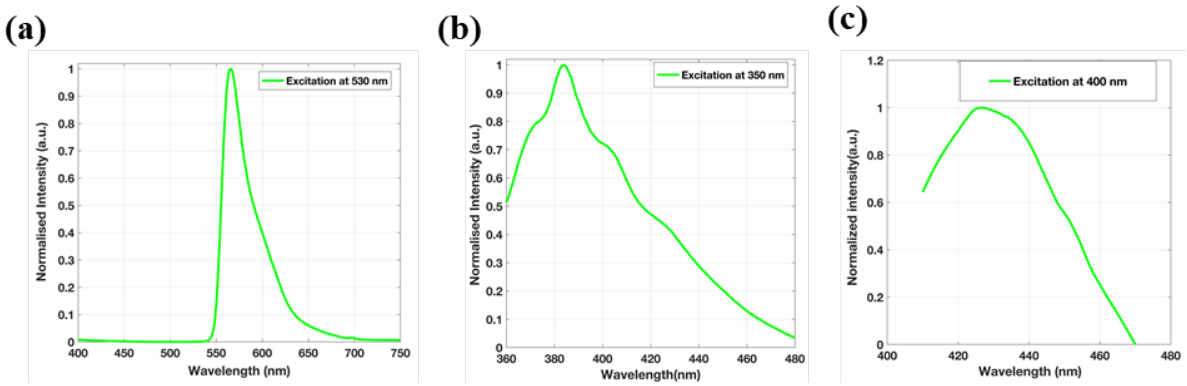

Figure 7.8: Emission spectra of Rhodamine 6G in ethanol with excitation at (a) 530 nm (b) 350 nm & (c) 400 nm

From the absorption and excitation spectrum, it is seen that apart from the absorption peak at 530 nm, there is absorption at 350 nm.

7.2.2.Pump – probe analysis

800nm pump was used for a TPE in Rhodamine 6G which would correspond to a state lying at 400nm from the ground state. Since, from the absorption and excitation spectrum it is clear that there is no significant OPA at 400 nm.

To study the TPA allowed states, pump – probe spectroscopy was used. Spectral traces for the same are shown in figure (7.9).

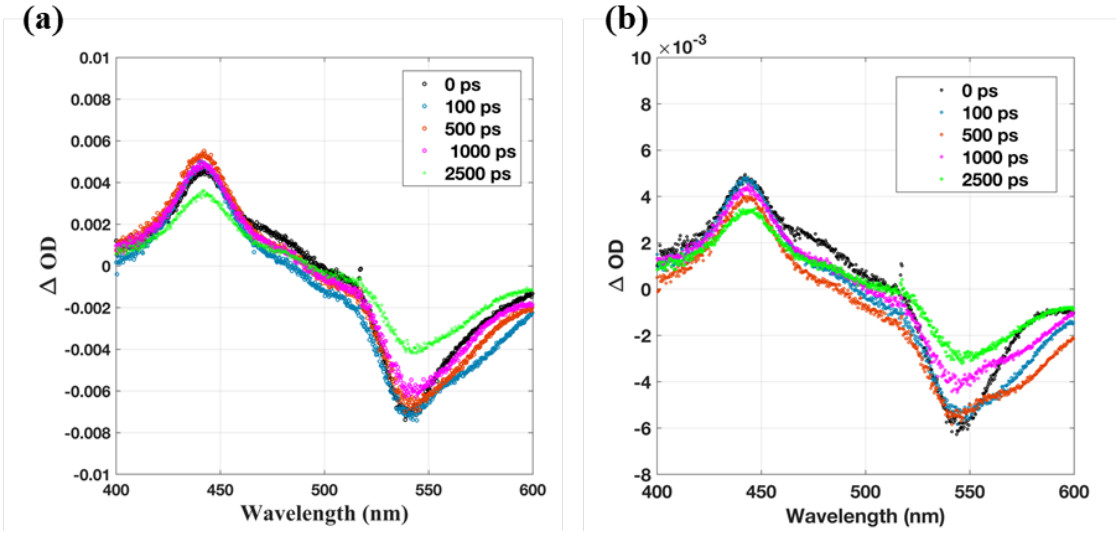

Figure 7.9: Transient absorption spectrum of Rhodamine 6G in (a) ethanol (b) ethylene glycol

From the transient absorption spectrum, it can be seen that there is an ESA signal centered at 440 nm and a SE signal centered on 540 nm. Also, it is seen that the spectrum relaxes much faster in ethylene glycol as compared to ethanol.

The kinetic traces at both these wavelengths were analyzed for both ethanol and ethylene glycol and are shown in figure (7.10) and figure (7.11).

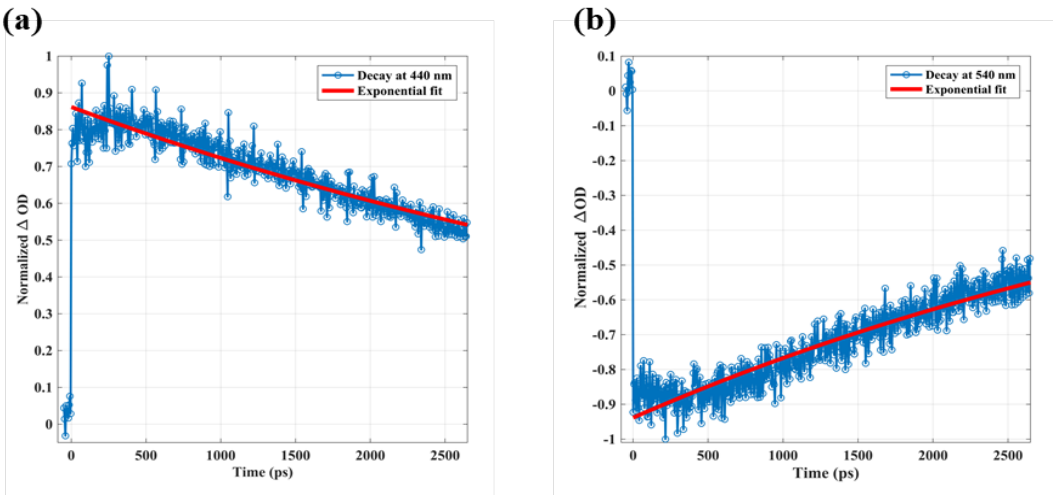

Figure 7.10: Kinetic traces for Rhodamine6G in ethanol for (a) ESA at 440nm (b) SE at 540nm

The kinetic decays were fitted to an equation of mono-exponential decay of type:

$$\mathbf{y = A \times \exp\left(\frac{-x}{t_1}\right)}$$

ESA at 440 nm			**SE at 540 nm**		
A	t_1 (ps)	R^2	A	t_1 (ps)	R^2
0.87	5704	0.86	0.94	4961	0.87

Table 7.2: Parameters for kinetic traces of Rhodamine6G in ethanol

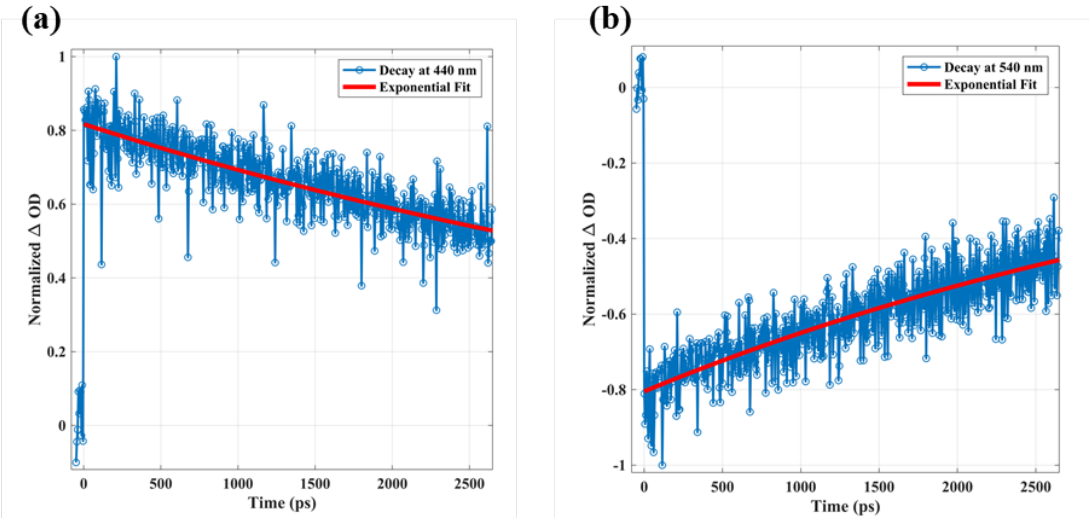

Figure 7.11: Kinetic traces for Rhodamine6G in ethylene glycol for (a) ESA at 440nm (b) SE at 540nm

ESA at 440 nm			**SE at 540 nm**		
A	t_1 (ps)	R^2	A	t_1 (ps)	R^2
0.82	6076	0.63	0.80	4674	0.70

Table 7.3: Parameters for kinetic traces of Rhodamine6G in ethylene glycol

Using pump – probe spectroscopy with 800 nm as pump and white light as probe, the dynamics of TPA induced transitions for Rhodamine 6G in two different solvents (ethanol and ethylene glycol) were studied.

Conclusion

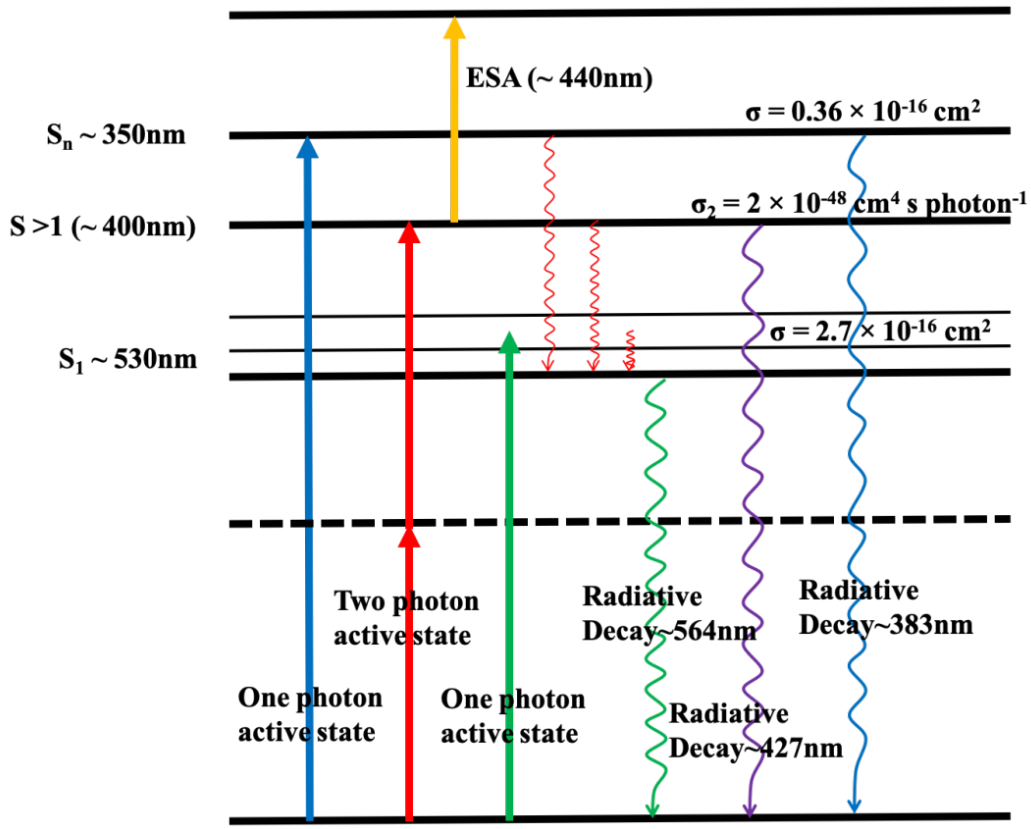

Figure 7.12: Electronic states of Rhodamine 6G

Figure (7.12) shows the different electronic states of Rhodamine 6G which have been explored using OPA and TPA. The values for the OPA cross sections and TPA cross section have been taken from reference [20].

BIBLIOGRAPHY

1. Rullière, *Femtosecond Laser Pulses* (2005).

2. R. W. Boyd, *Nonlinear Optics, 3rd edition* (2008).

3. DeLong, K. W., Trebino, R., Hunter, J., & White, W. E. (1994). Frequency-resolved optical gating with the use of second-harmonic generation. *Journal of the Optical Society of America B*, *11*(11), 2206–2215.

4. Zhang, Z., Wells, K. L., Hyland, E. W. J., & Tan, H.-S. (2012). Phase-cycling schemes for pump–probe beam geometry two-dimensional electronic spectroscopy. *Chemical Physics Letters*, *550*, 156–161.

5. Fuller, F. D., & Ogilvie, J. P. (2015). Experimental Implementations of Two-Dimensional Fourier Transform Electronic Spectroscopy. *Annual Review of Physical Chemistry*, *66*(1), 667–690.

6. De, A. K., Monahan, D., Dawlaty, J. M., & Fleming, G. R. (2014). Two-dimensional fluorescence-detected coherent spectroscopy with absolute phasing by confocal imaging of a dynamic grating and 27-step phase-cycling. *The Journal of Chemical Physics*, *140*(19), 194201.

7. Zhang, Z., Wells, K. L., Hyland, E. W. J., & Tan, H.-S. (2012). Phase-cycling schemes for pump–probe beam geometry two-dimensional electronic spectroscopy. *Chemical Physics Letters*, *550*, 156–161.

8. J.R. Lakowicz, *Principles of Fluorescence Spectroscopy* (2006).

9. Myers, J. A., Lewis, K. L. M., Tekavec, P. F., & Ogilvie, J. P. (2008). Two-color two-dimensional Fourier transform electronic spectroscopy with a pulse-shaper. *Optics Express*, *16*(22), 17420–17428.

10. P. Ogilvie, J., & J. Kubarych, K. (2009). Chapter 5 Multidimensional Electronic and Vibrational Spectroscopy: An Ultrafast Probe of Molecular Relaxation and Reaction Dynamics. In *Advances in Atomic, Molecular, and Optical Physics* (Vol. 57, pp. 249–321).

11. Warta, W., Stehle, R., & Karl, N. (1985). Ultrapure, high mobility organic photoconductors. *Applied Physics A*, *36*(3), 163–170.

12. Paci, I., Johnson, J. C., Chen, X., Rana, G., Popović, D., David, D. E., … Michl, J. (2006). Singlet Fission for Dye-Sensitized Solar Cells: Can a Suitable Sensitizer Be Found? *Journal of the American Chemical Society*, *128*(51), 16546–16553.

13. Smith, M. B., & Michl, J. (2010). Singlet Fission. *Chemical Reviews*, *110*(11), 6891–6936.

14. He, G. S., Tan, L.-S., Zheng, Q., & Prasad, P. N. (2008). Multiphoton Absorbing Materials: Molecular Designs, Characterizations, and Applications. *Chemical Reviews*, *108*(4), 1245–1330.

15. Wilson, M. W. B., Rao, A., Clark, J., Kumar, R. S. S., Brida, D., Cerullo, G., & Friend, R. H. (2011). Ultrafast Dynamics of Exciton Fission in Polycrystalline Pentacene. *Journal of the American Chemical Society*, *133*(31), 11830–11833.

16. He, G. S., Tan, L.-S., Zheng, Q., & Prasad, P. N. (2008). Multiphoton Absorbing Materials: Molecular Designs, Characterizations, and Applications. *Chemical Reviews*, *108*(4), 1245–1330.

17. Kaiser, W., & Garrett, C. G. B. (1961). Two-Photon Excitation in CaF_2: Eu^{+2}. *Physical Review Letters*, *7*(6), 229–231.

18. Xu, C., & Webb, W. W. (1996). Measurement of two-photon excitation cross sections of molecular fluorophores with data from 690 to 1050 nm. *Journal of the Optical Society of America B*, *13*(3), 481–491.

19. http://microscopy.berkeley.edu/courses/tlm/2P/index.html

20. Eggeling, C., Volkmer, A., & Seidel, C. A. M. (2005). Molecular Photobleaching Kinetics of Rhodamine 6G by One- and Two-Photon Induced Confocal Fluorescence Microscopy. *ChemPhysChem*, *6*(5), 791–804.

21. Megerle, U., Pugliesi, I., Schriever, C., Sailer, C. F., & Riedle, E. (2009). Sub-50 fs broadband absorption spectroscopy with tunable excitation: putting the analysis of ultrafast molecular dynamics on solid ground. *Applied Physics B*, *96*(2), 215–231.

LIST OF PUBLICATIONS

1. Yogita Silori, Pankaj Seliya and Arijit K. De (2019), Early time solvation dynamics probed by spectrally resolved degenerate pump-probe spectroscopy, *ChemPhysChem*, Accepted. http://dx.doi.org/10.1002/cphc.201900189

2. Pankaj Seliya, Yogita Silori and Arijit K. De (2018), Solvation Dynamics Probed by Two-Dimensional Electronic Spectroscopy, *PHOTONICS-2018: International Conference on Fiber Optics and Photonics (ISBN 978-93-88653-41-1)*, Paper No. SF2-C2.

3. Yogita Silori, Pankaj Seliya and Arijit K. De (2018), Early Time Solvation Dynamics Probed by Pump-Probe Spectroscopy, *PHOTONICS-2018: International Conference on Fiber Optics and Photonics (ISBN 978-93-88653-41-1)*, Paper No. FP155.